nature biomedical engineering

Article

https://doi.org/10.1038/s41551-022-00963-6

Generation of neural organoids for spinal-cord regeneration via the direct reprogramming of human astrocytes

Received: 1 September 2021

Accepted: 14 October 2022

Published online: 24 November 2022

Check for updates

Jinhong Xu[1,2,5], Shi Fang[1,2,5], Suixin Deng[1], Huijuan Li[1], Xiaoning Lin[3], Yongheng Huang[1,2], Sangmi Chung[4], Yousheng Shu[1] & Zhicheng Shao[1,2]

Organoids with region-specific architecture could facilitate the repair of injuries of the central nervous system. Here we show that human astrocytes can be directly reprogrammed into early neuroectodermal cells via the overexpression of *OCT4*, the suppression of *p53* and the provision of the small molecules CHIR99021, SB431542, RepSox and Y27632. We also report that the activation of signalling mediated by fibroblast growth factor, sonic hedgehog and bone morphogenetic protein 4 in the reprogrammed cells induces them to form spinal-cord organoids with functional neurons specific to the dorsal and ventral domains. In mice with complete spinal-cord injury, organoids transplanted into the lesion differentiated into spinal-cord neurons, which migrated and formed synapses with host neurons. The direct reprogramming of human astrocytes into neurons may pave the way for in vivo neural organogenesis from endogenous astrocytes for the repair of injuries to the central nervous system.

Three-dimensional (3D) human neural tissue loss after complete spinal-cord injury (SCI) is irreversible and often leads to functional paralysis of the lower limbs. Although regrowing 3D spinal-cord tissue is difficult[1–3], functional motor recovery of injured spinal-cord tissue in mice is possible after transplantation of multiple types of neural cell, including astrocytes[4], oligodendrocyte precursor cells[5], neural stem cells (NSCs) and neural progenitor cells (NPCs)[6–10] and neurospheres derived from human pluripotent stem cells (hPSCs)[11], indicating that cell transplantation is a promising therapeutic strategy for SCI. However, hPSC-derived cells would need to be further improved for use in potential clinical applications[12]. The engraftment of 3D constructs combining functionalized hydrogels with human NSC-derived cells from human fetal tissues has also improved behavioural recovery after SCI[13], yet fetal tissue is difficult to obtain and associated with ethical considerations. The spinal cord consists of spatially specialized neural tissue with different types of neuronal and glial cell, and developing spinal-cord-like tissue for the regeneration of SCI could be promising[14–16]. However, hPSC neurospheres and 3D-engineered hNSCs have not been induced into forming a specialized spinal-cord architecture.

Three-dimensional brain organoids from hPSCs are used to investigate neural development and neural diseases[17–24]. Previous studies have reported that 3D dorsal, intermediate and ventral developmental spinal-cord-like organoids were induced from hiPSCs using sonic hedgehog (SHH), bone morphogenetic protein 4 (BMP4) and fibroblast growth factor (FGF) morphogens[5,15]. Although patient-derived hiPSCs could be used to develop 3D organoids to avoid immune rejection, they need a well-defined neural differentiation protocol to eliminate non-neural cells and also require cell transplantation. In vivo direct reprogramming of endogenous glial cells is a promising approach for the regeneration of the central nervous system (CNS), as it would

[1]Institute for Translational Brain Research, State Key Laboratory of Medical Neurobiology, MOE Frontiers Center for Brain Science, Institute of Pediatrics, National Children's Medical Center, Children's Hospital, Fudan University, Shanghai, China. [2]Fujian Provincial Key Laboratory of Neurodegenerative, Disease and Aging Research, Institute of Neuroscience, School of Medicine, Xiamen University, Xiamen, Fujian, China. [3]Department of Neurosurgery, Zhongshan Hospital Xiamen University, Xiamen, Fujian, China. [4]Department of Cell Biology and Anatomy, New York Medical College, Valhalla, NY, USA. [5]These authors contributed equally: Jinhong Xu, Shi Fang. e-mail: zcshao@fudan.edu.cn

dispense with cell transplantation and avoid immunosuppression[25–28], and it has been shown via genetic manipulation or the use of small molecules that mouse and human astroglial cells can be efficiently converted into different kinds of functional postmitotic neurons in vitro and in vivo[26,28–37]. However, these induced neurons are not capable of proliferation and neural organogenesis. Therefore, the pre-eminent strategy for CNS repair is to induce brain organogenesis from endogenous astrocytes. A protocol for the efficient reprogramming of human astrocytes into 3D brain-region-specific organoids for CNS repair would thus be useful.

Here we present a method for the generation of 3D brain organoids via the direct reprogramming of human astrocytes by leveraging *OCT4* (O) and *p53* genes and the small-molecule cocktail CHIR99021 (C), SB431542 (SB), RepSox (R) and Y27632 (Y) (termed Op53-CSBRY). Human astrocytes treated with Op53-CSBRY were directly reprogrammed into neural ectodermal cells that further generated human-astrocyte-derived organoids (hAD-Organs). These hAD-Organs can be patterned into spinal-cord organoids by activating FGF, SHH and BMP signalling. The grafts of human-astrocyte-derived spinal-cord organoids (hADSC-Organs) survived, differentiated into spinal-cord neurons, sprouted long-distance axons, formed synaptic connectivity with host neurons and provided protective effects in mice with complete SCI.

Results

Op53-CSBRY efficiently converted human astrocytes into neurons

Direct reprogramming of primary glial or fibroblast cells yields postmitotic neurons that cannot proliferate or form adequate cytoarchitectural CNS tissue in vitro or in vivo, which is a major disadvantage for the regeneration of CNS tissue after brain damage[30,34,36,38]. The number of converted neurons largely depends on the expandability and non-senescent quality of the donor somatic cells, as well as on the reprogramming efficiency. To obtain proliferative neural cells and trigger organogenesis, we hypothesized that the master reprogramming factor *OCT4* may enhance the human astrocyte reprogramming process[39,40] and that the reduction of the cell-cycle regulator *p53* may promote the proliferation of intermediate reprogrammed cells[41–43]. We first overexpressed *OCT4* and knocked down *p53* synchronously in human primary astrocytes (hereinafter referred to as Op53). It was found that only a few astrocytes could be reprogrammed into MAP2$^+$ cells (Supplementary Fig. 1a), although astrocytes had demonstrated *OCT4* overexpression and *p53* knockdown efficiently (Supplementary Fig. 1b,c). To improve the astrocyte conversion efficiency, we selected 15 small molecules involved in neural differentiation or somatic cell reprogramming. The 15 small molecules for primary screening were CHIR99021, valproic acid, Y27632, SB431542, XAV939, forskolin, JQ1, PD0325901, RepSox, Isoxazole 9 (ISX-9), LDN193189, arotiniod acid (TTNPB), smoothened agonist (SAG), SU5402 and gamma-secretase inhibitor (DAPT). Through single small-molecule screening (initial screening protocol; Fig. 1a,b), we found that the efficiencies of human astrocyte reprogramming into MAP2$^+$ neurons increased substantial (>8%) when treated with CHIR99021, SB431542, RepSox and Y27632 (Fig. 1c,d). MAP2$^+$ neuronal clusters were also observed (Supplementary Fig. 1d) in these four groups, which indicated that astrocytes may transiently re-enter the cell cycle and that they proliferated during the reprogramming process. To further enhance the reprogramming efficiency, we then tested different combinations of these four small molecules. We found that CHIR99021, SB431542, RepSox and Y27632, taken together (CSBRY), robustly increased the astrocyte conversion efficiency (Fig. 2a,b). To further confirm this human astrocyte reprogramming method, we generated developmental astrocytes from human embryonic stem cells (hESCs) (Supplementary Fig. 2a). About 96% of hESC-derived astrocytes expressed glial fibrillary acidic protein (GFAP) during this differentiation process (Supplementary Fig. 2b). hESC-derived astrocytes were reprogrammed into MAP2$^+$ neurons with a significant efficiency similar to primary astrocytes treated with Op53-CSBRY (Fig. 2c,d). To further confirm the results for the human fetal astrocytes, we collected mature astrocytes containing >80% of GFAP-positive astrocytes from three patients (aged between 13 and 65 years) with gliomas (Supplementary Fig. 2c). Astrocytes from the patient samples (2/3) were effectively reprogrammed into neurons, but with much lower efficiency than human fetal astrocytes (Fig. 2e,f), indicating that different developmental stages of astrocytes may affect the reprogramming efficiency. Taken together, these results show that human astrocytes can be robustly reprogrammed into neurons by Op53-CSBRY in vitro.

Reprogramming of human astrocytes into cerebral organoids via Op53-CSBRY

We treated commercially acquired primary astrocytes isolated from the cerebral cortex of healthy human brains with Op53-CSBRY. We observed that Op53-CSBRY induced many rosette-like clusters at day 14 (Extended Data Fig. 1a). This may suggest that primary astrocytes re-enter neurogenesis during reprogramming. To confirm this hypothesis, we transferred these reprogrammed cells into a suspension-culture system (Fig. 3a,b). After suspension at day 14, the induced cells were aggregated as spherical structures (Fig. 3c). After being embedded in Matrigel, the spheroids showed neuroepithelial buds. The size of the spheroids was about 3 mm at day 90 (Fig. 3c) and reached 4–5 mm when the spheroids were cultured over 15 weeks (Extended Data Fig. 1b), which is similar to the size of cerebral organoids derived from hPSCs[21,44]. After 7 weeks of culture, we observed the neural progenitor cell marker SOX2$^+$ and PAX6$^+$ ventricular-zone-like (VZ-like) structures, including a TUJ1$^+$/MAP2$^+$ neuronal layer[21] (Fig. 3d and Extended Data Fig. 1c,d). SOX2$^+$ and PAX6$^+$ VZ regions were continually enlarged at 10 weeks (Fig. 3e). To investigate whether these hAD-Organs include multiple cortical layers, we performed immunostaining to examine protein expression with different cortical layer markers (Fig. 3f). We found that the deep cortical layer marker CTIP2$^+$ and TBR1$^+$ cells were mainly distributed on the outside of the PAX6$^+$ VZ region. The superficial layer neuronal markers SATB2$^+$ and BRN2$^+$ were located at the intermediate layers and were separated from Reelin$^+$ cells, which resembled the layer-I marginal zone of the cerebral cortex (Fig. 3g and Extended Data Fig. 1e,f). These results indicated that hAD-Organs might have formed the structure of six cortical layers at week 10. In addition, Op53 treatment alone was not sufficient to support astrocyte reprogramming to form hAD-Organs (Fig. 3h,i and Supplementary Fig. 3a). Treatment with CSBRY induced rapid cell proliferation over 240-fold compared with the control at day 42 (Fig. 3h) and showed typical cerebral organoids with larger neuroepithelial buds than in the control (Fig. 3i and Supplementary Fig. 3a). Immunostaining and fluorescence-activated cell sorting (FACS) assays revealed that the majority of cells in the hAD-Organs were TUJ1$^+$/MAP2$^+$ cells showing typical neuronal morphology in the CSBRY-treated group (Fig. 3j,k and Supplementary Fig. 3b). These findings indicated that the CSBRY cocktail robustly induced and accelerated the growth and proliferation of organoids during human astrocyte conversion.

To identify the origin of hAD-Organs in our reprogramming system, primary cultures of human astrocytes were analysed by immunostaining and a neurosphere assay. More than 80% of human primary astrocytes co-expressed *GFAP* and *S100β*, with almost no MAP2$^+$ neurons (Extended Data Fig. 2a,b). However, some NPCs with weak expression of *SOX2* and *PAX6* were found in the cultured human fetal astrocytes (Extended Data Fig. 2a,b). To test the ability of neurogenesis in these cells, we seeded 50 primary astrocytes per well into an ultralow-attachment 24-well plate with the neurosphere culture medium containing basic fibroblast growth factor (bFGF) and epidermal growth factor (EGF). After 14 days, we found that neurospheres were generated from the Op53-CSBRY reprogrammed astrocytes, but none were generated from the primary cultured astrocytes (Extended

https://doi.org/10.1038/s41551-022-00963-6

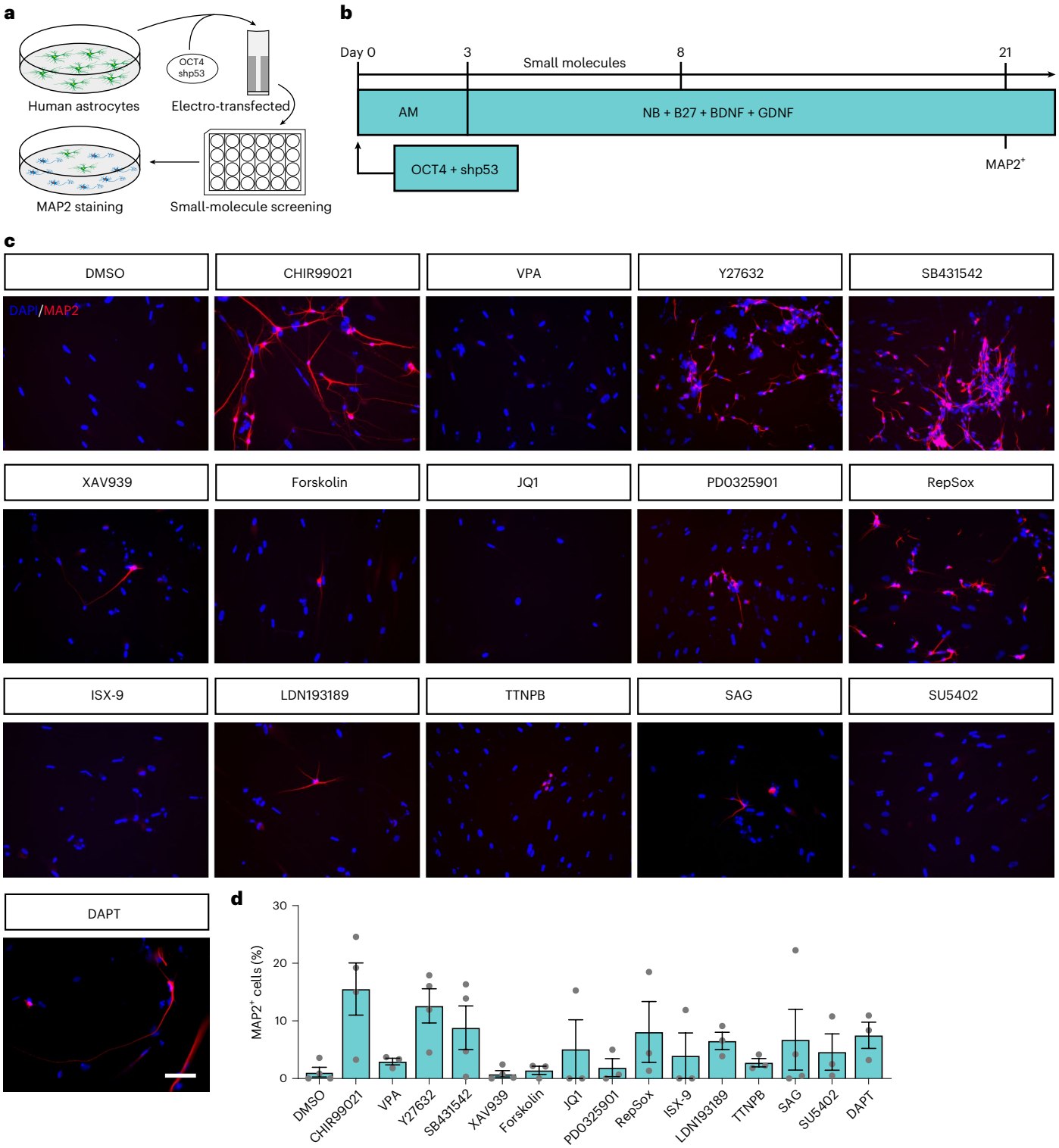

Fig. 1 | Small-molecule screening to improve the efficiency of astrocyte-to-neuron conversion. a, Schematic of the direct reprogramming of human astrocytes into neurons. **b**, Diagram of the primary screening protocol for the conversion of human astrocytes into neurons using each of the 15 small molecules. AM, astrocyte medium; NB, neurobasal medium. **c**, Representative images of MAP2$^+$ cells treated with each of the 15 small molecules and dimethyl sulfoxide (DMSO) as control at day 21. Scale bars, 100 µm. VPA, valproic acid. **d**, Quantification of the percentage of induced MAP2$^+$ neurons treated with the 15 small molecules (CHIR99021, Y27632, SB431542, XAV939 and SAG, $n = 4$ independent experiments; the rest, $n = 3$ independent experiments) and DMSO ($n = 4$ independent experiments). Data are presented as mean ± standard error of the mean (s.e.m.).

Data Fig. 2c), indicating that the contaminated SOX2$^+$ and PAX6$^+$ cells in primary human astrocytes were not bona fide NSCs and that they had lost the ability of neurogenesis after long-term culture in the serum-containing medium. In addition, we could not find MAP2$^+$ cells in cultured primary human astrocytes treated with the small molecules ISX-9 and retinoic acid (RA), which were used to induce the neural differentiation of NSCs (Extended Data Fig. 2d). Furthermore, astrocytes treated with Op53 alone could not generate brain

https://doi.org/10.1038/s41551-022-00963-6

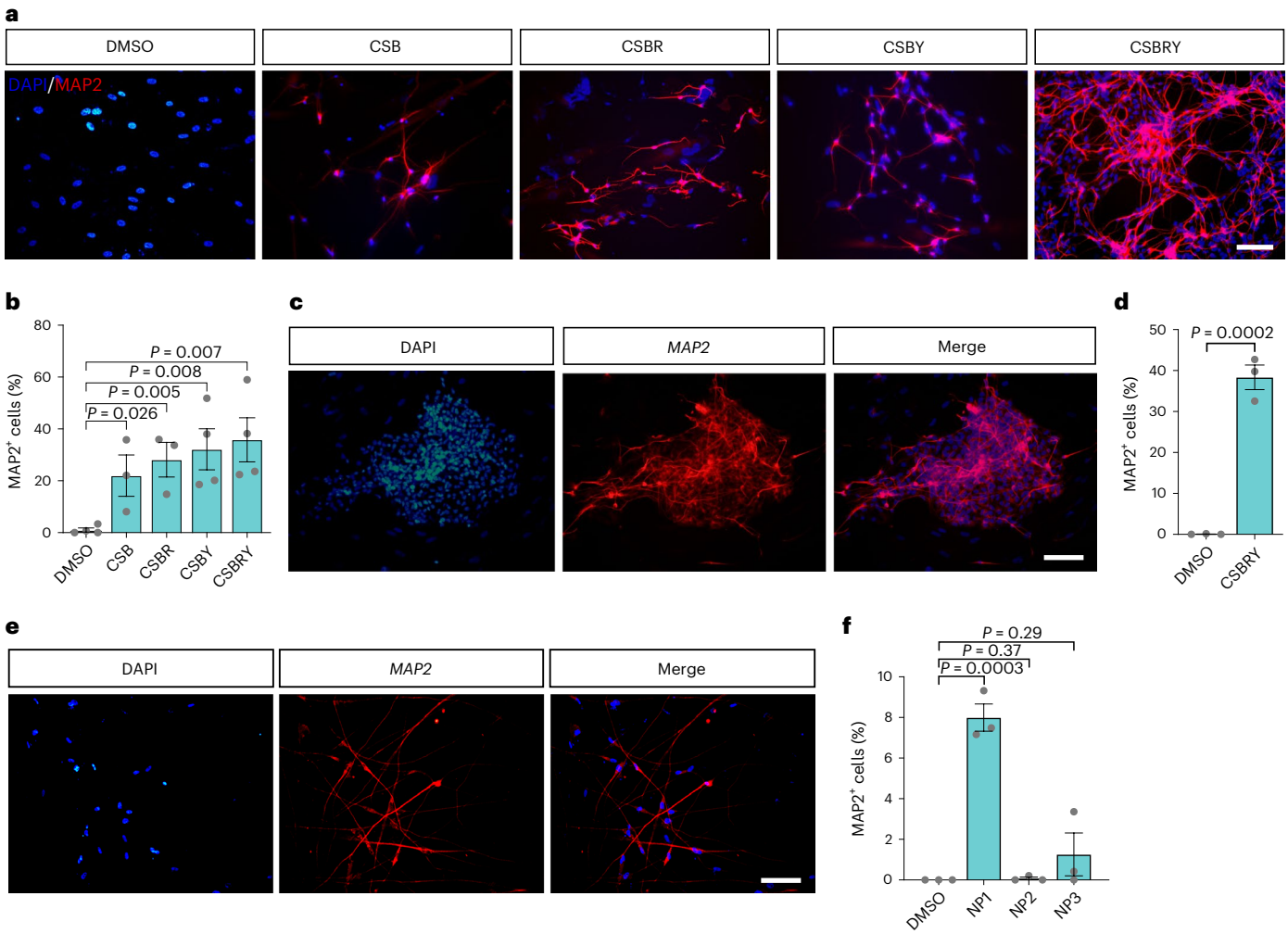

Fig. 2 | Conversion of human astrocytes into neurons using Op53-CSBRY. a, Representative images of MAP2$^+$ cells treated with different combinations of small molecules and DMSO. Scale bars, 100 µm. **b**, Quantitative analysis of MAP2$^+$ cells treated with small-molecule combinations (CSBY and CSBRY groups, $n = 4$ independent experiments; the rest, $n = 3$ independent experiments) and DMSO ($n = 4$ independent experiments). **c**, Representative images of MAP2$^+$ neurons converted from hESC-derived astrocytes treated with the CSBRY cocktail. Scale bars, 100 µm. **d**, Quantitative analysis of MAP2$^+$ neurons converted from hESC-derived astrocytes treated with CSBRY ($n = 3$ independent experiments). **e**, Representative images of MAP2$^+$ neurons converted from human mature astrocytes isolated from patients with glioma and treated with the CSBRY cocktail. Scale bars, 100 µm. **f**, Quantitative analysis of MAP2$^+$ neurons converted from human mature astrocytes isolated from patients with glioma and treated with CSBRY ($n = 3$ independent experiments). NP, patient with glioma. Data are presented as mean ± s.e.m. An unpaired Student's *t*-test was used to compare the two groups.

organoids (Fig. 3h,i and Supplementary Fig. 3a). These results indicated that CSBRY was necessary for the generation of hAD-Organs in this astrocyte reprogramming system. To trace the origin of the induced neurons, we infected human astrocytes with human glial fibrillary acidic protein promotor controlling expression of enhanced green fluorescent protein (hGFAP::EGFP) AAV virus. We found that most of the cells showed EGFP expression manifesting their astrocytic identities. Some of the EGFP$^+$ cells showed neuronal morphology when treated with CSBRY at day 19 and co-expressed *MAP2*, representing their neuronal identities (Extended Data Fig. 2e). Time-lapse imaging showed that EGFP$^+$ astrocytes with flat morphology divided and converted into neuron-like cells (Extended Data Fig. 2g and Supplementary Video 1). After time-lapse imaging, we fixed the cells and found that the neuron-like cells were MAP2$^+$ with weak expression of EGFP, suggesting that the converted neurons originated from human astrocytes (Extended Data Fig. 2e,f). In hGFAP::EGFP-labelled cortical organoids at week 3, we found that some of the *GFP*-positive cells were co-labelled with MAP2$^+$ neurons and that some GFP$^+$ cells were FOXG1$^+$ or SOX2$^+$ NPCs, but most of them still maintained their astrocytic identities (S100β$^+$) (Extended Data Fig. 1g–k). To further characterize the origin and cell population of the initial cultured human astrocytes that were isolated from the human fetal cerebral cortex, we conducted single-cell RNA sequencing and identified these astrocytes on the basis of cortical-astrocyte-layer-specific markers, which were recently reported via a single-cell in situ transcriptomic map in the cerebral cortex[45]. We did not observe OCT4$^+$, NANOG$^+$ and LIN28A$^+$ hESCs or NeuN$^+$ and DCX$^+$ neurons (Extended Data Fig. 3a–c). The majority of the primary astrocytes expressed cortical upper grey matter astrocyte markers (such as 84.2% *ITM2B*, 88.8% *BSG* and 81.6% *IGFBP2*), and over 50% of the cells expressed deeper-layer astrocyte markers (57.3% *ID1*, 55.1% *ID3*, 58.7% *DKK3* and 57.6% *EFHD2*), indicating that they developed cortical grey matter astrocyte identities (Extended Data Fig. 3a,d–f). Taken together, these data suggested that hAD-Organs were generated from developing human cortical astrocytes reprogrammed by Op53-CSBRY and not from contamination by NPCs. Finally, our results verified that human primary astrocytes could be directly reprogrammed into hAD-Organs by Op53-CSBRY in vitro.

https://doi.org/10.1038/s41551-022-00963-6

Generation of spinal-cord organoids derived from human astrocytes

Previous studies reported that FGF, SHH and BMP4 morphogens were involved in patterning spinal-cord tissue during development[9,15]. It is not known whether these Op53-CSBRY-induced astrocytes could respond to spinal-cord patterning signals. To confirm this, we designed a protocol for treating Op53-CSBRY-induced astrocytes with bFGF, SAG and BMP4 to develop hADSC-Organs (Fig. 4a,b). After 4-week induction, hADSC-Organs grew up to about 1 mm, and the size robustly increased to 2–3 mm after 7 weeks (Fig. 4c). We then performed immunostaining with different dorsal and ventral spinal-cord progenitor markers (Fig. 4d). We observed that *PAX6*, the ventral progenitor domain markers *Nkx6.1* and *Olig2* and the dorsal progenitor domain marker *Olig3* were highly expressed in these hADSC-Organs (Fig. 4e–h and Extended Data Fig. 4a,b). Specifically, Nkx6.1$^+$ cells formed the VZ-like structure (Fig. 4e,f and Extended Data Fig. 4a), and dorsal Olig3$^+$ cells were well separated from ventral Nkx6.1$^+$ cells (Fig. 4h). Furthermore, Olig2$^+$ ventral motor NPCs mainly clustered and co-localized with Nkx6.1$^+$ cells (Fig. 4f). These results show that this protocol induced both ventralized and dorsalized progenitor identities of the developing spinal cord.

Next, we examined whether hADSC-Organs could generate different subtypes of spinal-cord neuron. Notably, TUJ1$^+$/MAP2$^+$ neurons and ChAT$^+$ or HB9$^+$ spinal-cord-specific motor neurons were detected in 10-week-old hADSC-Organs (Fig. 4i,j and Extended Data Fig. 4c,d). Major neuronal subtype GAD67$^+$ inhibitory interneurons and VGLUT1$^+$ excitatory neurons were observed to be in this stage (Fig. 4k,l). The populations of neurons showed 42.9 ± 15.9% MAP2$^+$ and 40.1 ± 19.0% TUJ1$^+$ neurons. Some of the cells expressed the spinal-cord motor neuron marker *ChAT* (38.7 ± 11.4%) and *HB9* (24.4 ± 7.5%) (Extended Data Fig. 4e). VGLUT1$^+$ and GAD67$^+$ neurons were 26.1 ± 11.6% and 34.2 ± 6.7%, respectively, in 10-week-old hADSC-Organs (Extended Data Fig. 4e). To better characterize hADSC-Organs, we dissociated and plated the 10-week-old hADSC-Organs. After plating for 5 days, most of the cells displayed typical neuronal morphology and only a few GFAP$^+$ cells (Extended Data Fig. 4f–h), and ChAT$^+$ spinal-cord motor neurons showed high co-expression with *MAP2* (Extended Data Fig. 4i). To further confirm human developmental spinal-cord identities, we measured the global transcriptome of hADSC-Organs compared with that for hAD-Organs by RNA sequencing analyses. At week 7, hAD-Organs showed high expression of cortical progenitor marker genes. In contrast, human developmental spinal-cord-specific transcriptional genes, such as the HOX family genes *MNX1*, *ISL1*, *ChAT*, *LHX3*, *NKX2.2* and *NKX6.1*, were robustly expressed in hADSC-Organs (Extended Data Fig. 4j,k). Gene ontology analysis revealed the enrichment of many spinal-cord developmental biological processes in 7-week-old hADSC-Organs, such as anterior/posterior pattern specification, and sensory perception of pain (Extended Data Fig. 4l).

To further investigate the spinal-cord identities of hADSC-Organs, we performed single-cell RNA sequencing for hADSC-Organs. We found that cells in hADSC-Organs were grouped into 17 main clusters; we then characterized the dorsal and ventral domain-specific cell populations and gene expression profiles according to the reported markers of developmental spinal cord[5,46]. We found that 7-week-old hADSC-Organs contained two main types of cell: spinal-cord domain-specific neural progenitors and subtype neurons (Fig. 5a–c). The neural progenitors represented about 41.15% of the total number of cells and could be subdivided into RP, dp1, dp2–6, p0/1, p2, pMN and p3/FP progenitor regional clusters, whereas the neuronal cells (58.83%) contained dI1, dI2–6, V0/1, V2, MN and V3 spinal-cord regional cell clusters (Fig. 5b). Cluster p0/1 had the largest proportion of progenitor clusters (18.18%). Cluster V0/1 (19.43%) and MN (19.29%) had the two largest proportions of neuronal cells in 7-week-old hADSC-Organs. Bubble charts in Fig. 5c depict the well-expressed pattern of spinal-cord dorsal and ventral domain-specific markers in each assigned cell cluster, indicating their developmental spinal-cord identities (Fig. 5c). In addition, *SOX2* and the neural markers *MAP2* and *TUBB3* were highly expressed in 7-week-old hADSC-Organs (Fig. 5f). The spinal-cord motor neuron markers *MNX1* and *ISL1* were shown in similar neuronal clusters, but different with GATA3$^+$ V2 interneurons (Fig. 5f). Furthermore, we found that GABAergic neurons (GAD1$^+$, SLC32A1$^+$ and GAD2$^+$) were broadly expressed in multiple cell clusters and that glutamatergic (SLC17A6$^+$), glycinergic (SLC6A5$^+$) and cholinergic (SLC5A7$^+$ and SLC18A3$^+$) subtype neurons were found in different specific domains (Fig. 5d). We also found the increased expression of *HOXA2*–*HOXA5*, *HOXB2*–*HOXB8*, *HOXC4*, *HOXC5*, *HOXD3* and *HOXD4* in hADSC-Organs, representing caudal cervical/thoracic spinal-cord identities (Fig. 5e). Hence, our results show that hADSC-Organs possess developing spinal-cord identities with dorsoventral and rostrocaudal spatial cytoarchitectures.

In summary, under in vitro defined conditions, we induced human astrocytes into spinal-cord organoids that included human ventral and dorsal spinal-cord progenitors and major neuronal subtypes and that resembled human developmental spinal-cord-like tissue.

Transcriptional analysis of neurons converted from human astrocytes

To understand the mechanisms of the direct reprogramming of human commercial astrocytes into 3D organoids, we performed RNA sequencing for the analysis of transcriptional profiles after 5 days of CSBRY treatment. A sample distance matrix showed that the three independent biological replicates treated by CSBRY were well clustered (Extended Data Fig. 5a). Compared with control treatments, 2,250 genes had significant differential expression ($pVal < 0.05$, $\log_2$Fold Change (FC) > 1, Fig. 6a,b). Differentially expressed genes (71.2%) were upregulated by CSBRY. In contrast, only 28.8% of the differentially expressed genes were downregulated (Fig. 6b and Extended Data Fig. 5b). Over 30% of differentially expressed genes, including both upregulated and downregulated genes, were involved in signal transduction by the Kyoto Encyclopedia of Genes and Genomes (KEGG) pathway enrichment assay (Extended Data Fig. 5c). These results indicated that the CSBRY chemical cocktail mainly activated the external signalling pathways during the reprogramming process. We also found that CSBRY treatment significantly upregulated the expression of the embryonic stem

Fig. 3 | 3D cortical organoids generated from Op53-CSBRY-treated human astrocytes. a, Schematic illustrating the generation of human cortical organoids from human astrocytes. **b**, Diagram of the protocol for inducing 3D cortical organoids. **c**, Representative images of cortical organoids induced from human astrocytes by Op53-CSBRY at days 8, 14, 42 and 90. Scale bars, 100 µm (day 8), 400 µm (day 14) and 1,000 µm (days 42 and 90). **d**, Immunostaining of sections from cortical organoids at week 7 using neuronal markers *TUJ1* and *MAP2* (left), *TUJ1* and neural progenitor marker *PAX6* (middle) and neural progenitor marker *SOX2* and neuronal marker *MAP2* (right). Scale bars, 25 µm (left), 50 µm (middle) and 25 µm (right). **e**, Immunostaining of sections from cortical organoids at week 10 using *TUJ1* and *MAP2* (left), *TUJ1* and *PAX6* (middle) and *SOX2* and *MAP2* (right). Scale bars, 50 µm. **f**, Schematic representation of the neuronal markers for genes expressed in the six cortical layers (I–VI). **g**, Representative immunostained sections from cortical organoids with *PAX6* and the cortical layer markers (from left to right: *CTIP2*, *SATB2*, *TBR1* and *BRN2* and from second left to right: *Reelin*) at day 70. The dotted line delineates the VZ-like structures. Scale bars, 25 µm. **h**, Quantitative analysis showed that treatment with CSBRY induced rapid proliferation compared with only the Op53/DMSO control ($n = 3$ independent experiments). 'Fold' is the fold change in cell number compared with the control. Data are presented as mean ± s.e.m. **i**, Representative images of hAD-Organs induced by the Op53/DMSO control and by Op53-CSBRY ($n = 3$ independent experiments). Scale bar, 1,000 µm. **j**, Immunostaining showed that 7-week-old hAD-Organ-dissociated cells were MAP2$^+$ and TUJ1$^+$ neurons. Scale bar, 25 µm. **k**, Quantitative analysis of the percentage of MAP2$^+$ and TUJ1$^+$ neurons dissociated from 7-week-old hAD-Organs treated by Op53-CSBRY ($n = 3$ independent experiments). Data are presented as mean ± s.e.m.

https://doi.org/10.1038/s41551-022-00963-6

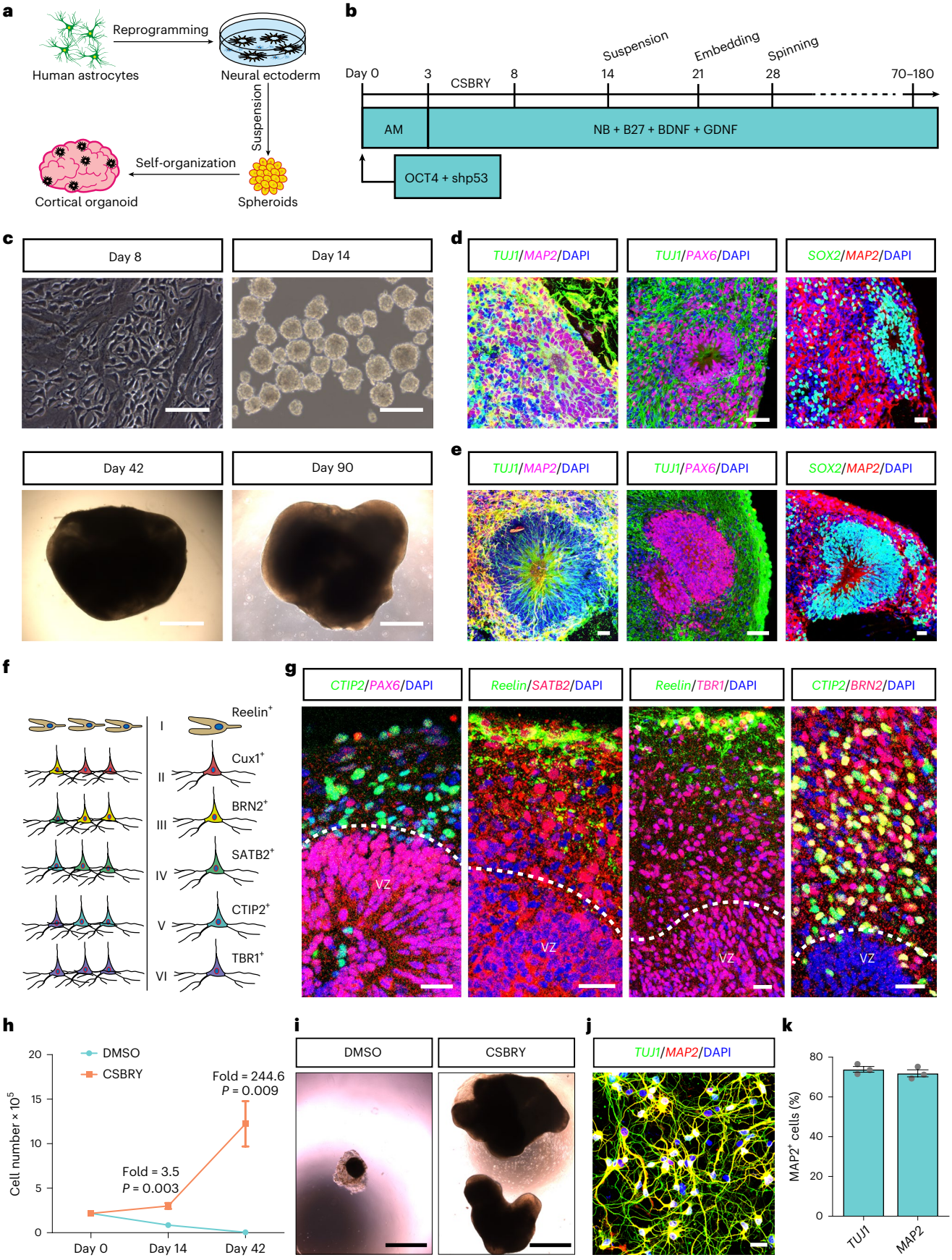

https://doi.org/10.1038/s41551-022-00963-6

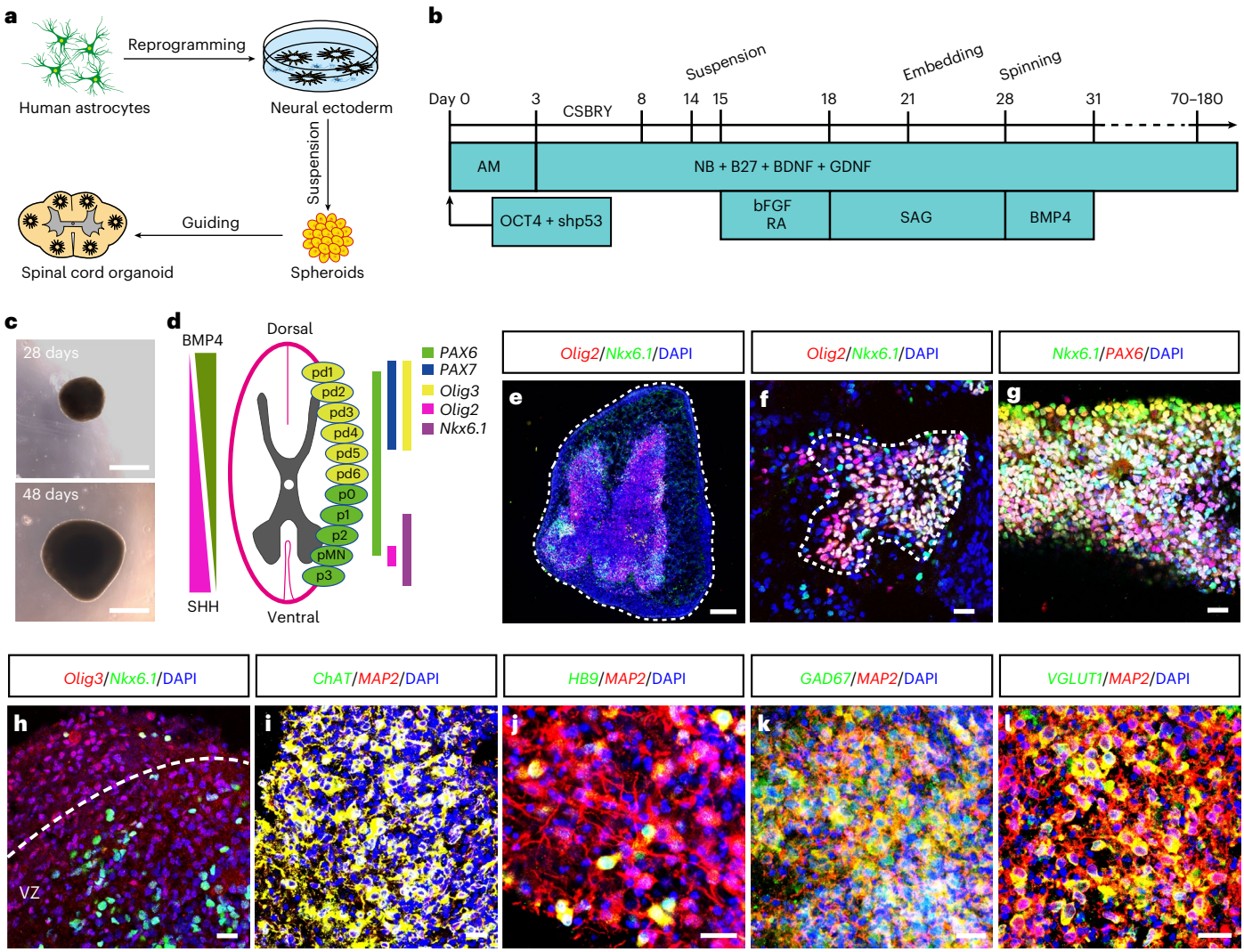

Fig. 4 | Generation of hADSC-Organs. a, Schematic illustrating the generation of human spinal-cord organoids from human astrocytes. **b**, Diagram of the induction of hADSC-Organs. **c**, Phase images of hADSC-Organs at different stages. Scale bars, 1,000 µm. **d**, Diagram showing the expression pattern of dorsal (pd1–pd6) and ventral progenitor domain markers (p0–p3) in the developing spinal cord. Left: BMP4 and SHH concentration gradients. Right: transcription factors expressed by the domains. **e**–**h**, Representative immunohistochemistry images of sections from hADSC-Organs at week 7, showing a high expression of *Nkx6.1* and *Olig2* in low-power (**e**) and high-power (**f**) images, *PAX6* co-localization with *Nkx6.1* (**g**) and *Olig3* well separated from Nkx6.1$^+$ cells (**h**). Dotted lines delineate the VZ area. Scale bars, 500 µm (**e**) and 25 µm (**f**–**h**). **i**–**l**, Immunostaining of sections from hADSC-Organs at week 10 characterizing the specific cholinergic spinal-cord motor neuron markers *ChAT* (**i**) and *HB9* (**j**), *GAD67*-positive GABAergic interneurons (**k**) and *VGLUT1*-positive glutamatergic neurons (**l**). Scale bars, 25 µm. Representative images from three sections of hADSC-Organs with similar results (**e**–**h**, **i**–**l**).

cell marker genes *SOX2*, *LIN28A* and *SALL4* (Fig. 6c). However, overexpressed *OCT4* was downregulated, and another key pluripotent gene *NANOG* was not activated (Fig. 6c). We also found that other embryonic regulation genes, such as *UTF1*, *ZFP42*, *TBX3*, *RIF1* and *FZD1*, showed no activation (and even downregulation). The human pluripotent stem cell markers NANOG$^+$, SEEA4$^+$ and TRA-1-60$^+$ cells were not observed in primary cultured astrocytes or in Op53-CSBRY-induced cells (Extended Data Fig. 5g). These results suggested that human astrocytes were not reprogrammed into full pluripotent stem cells by Op53-CSBRY. We found that specific neural ectodermal genes, such as *OTX2*, *NOG*, *SOX1*, *FGF8*, *NES* and *PAX6*, were significantly upregulated (Fig. 6d). However, the surface ectodermal genes *MSX1* and *MSX2* were significantly downregulated (Fig. 6e). In addition, mesodermal and endodermal gene expressions were not activated (Fig. 6f,g). These data suggested that induced cells possessed neural ectodermal characteristics. Gene ontology pathway analysis showed that differential expressions were significantly enriched in biological processes, including cell proliferation in the forebrain, cell fate commitment and nervous system development (Fig. 6h). To further confirm their neural ectodermal cellular identities, we found that cultured human astrocytes have almost no *OTX2* expression but low expression of *FOXG1*, *SOX2* and *NES* (Fig. 6c,d,j,k and Extended Data Fig. 5e,f). However, CSBRY treatment robustly increased *SOX2*, *SOX1*, *LIN28A*, *SALL4*, *OTX2*, *GBX2*, *FGF8*, *NES* and *PAX6* expression; most of them showed high expression in neural ectodermal cells, and some of the induced cells highly co-expressed *FOXG1* and *OTX2* in one rosette-like cluster (Fig. 6c,d,l–n and Extended Data Fig. 5e,f), indicating that human astrocytes were actually reprogrammed by Op53-CSBRY into early neural ectodermal cells with heterogeneous characteristics, which may show different regional identities of the neural tube (Fig. 6m,n). In summary, these results suggested that human astrocytes treated with Op53-CSBRY were directly reprogrammed into early neuroectodermal cells, which were amenable for regional specification and expansion (Fig. 6i). The cancer gene *p53* was not continually downregulated, and the cancer genes *KLF4* and *MYC* were

https://doi.org/10.1038/s41551-022-00963-6

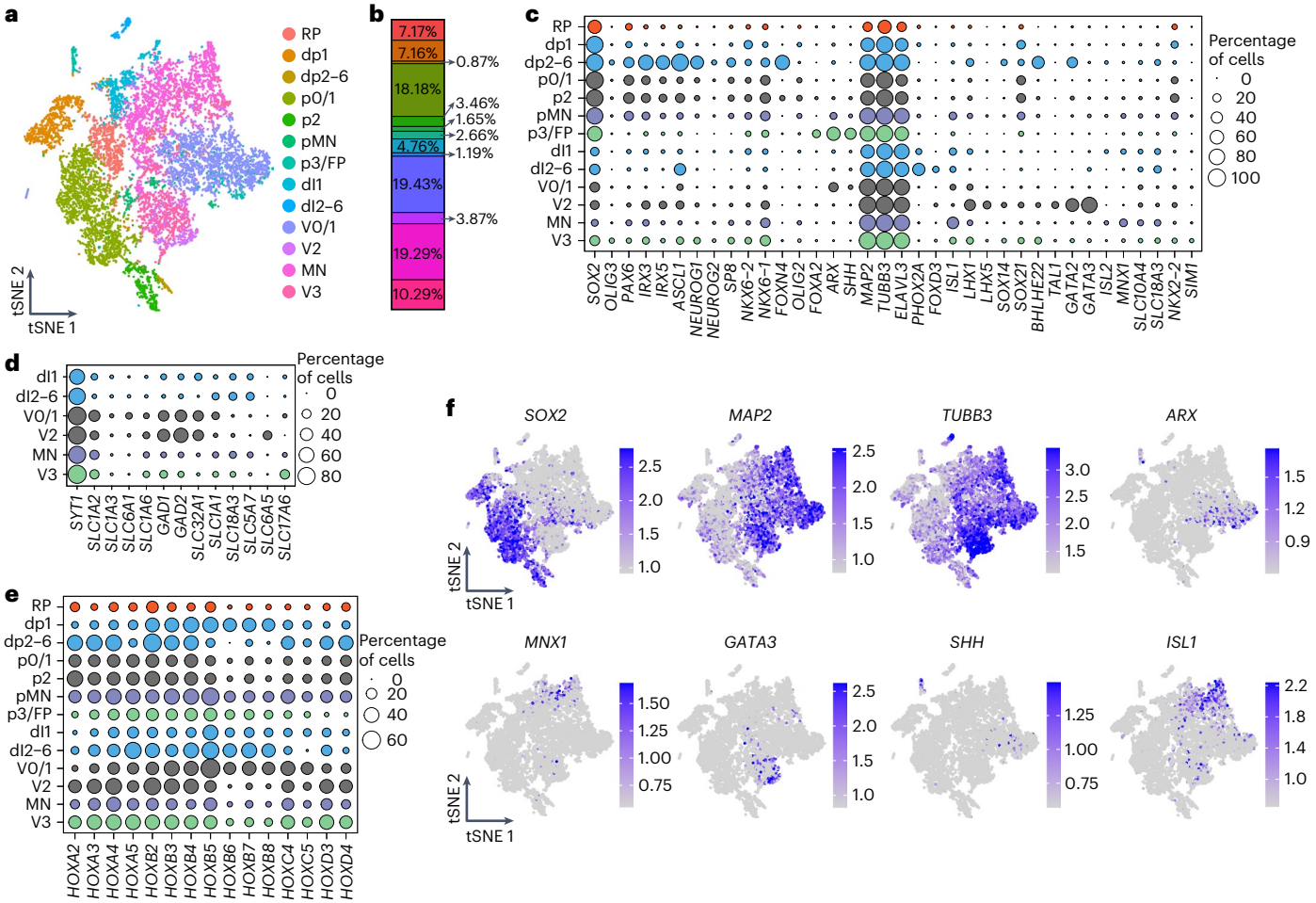

Fig. 5 | Transcriptome profiling of hADSC-Organs. a, T-distributed stochastic neighbor embedding explained (tSNE) visualization of single-cell gene expression of hADSC-Organs at day 49 (n = 12,341, cells from 4 hADSC-Organs). RP, roof plate; dp1–6, dorsal progenitor cell types; p0–3, ventral progenitor cell types; pMN, motor neuron progenitors; FP, floor plate; dI1–6, dorsal interneurons; V0–3, ventral neurons; MN, motor neuron. **b**, Percentage of cells in each cluster in hADSC-Organs. **c**–**e**, Bubble charts showing the expression of selected domain-specific markers used to identify dorsal and ventral domain progenitors and neuronal subtypes (**c**), neurotransmitter identity-related genes in neuronal clusters (**d**) and HOX family genes in each cluster in hADSC-Organs (**e**). **f**, tSNE plots showing the gene expression of selected hADSC-Organ neural progenitors, neuron markers and motor neuron progenitors. The colour scale shows normalized gene expression levels.

not activated by CSBRY treatment (Extended Data Fig. 5d), suggesting a low ability to induce cancer. Taken together, Op53-CSBRY directly reprogrammed human astrocytes into early neuroectodermal cells, enabling the patterning of region-specific brain organoids by neural morphogens.

Functional characterization of hAD-Organs and hADSC-Organs

We next investigated whether the induced neurons were functional. We performed whole-cell electrophysiological recordings from dissociated both hAD-Organs and hADSC-Organs (Fig. 7 and Extended Data Fig. 6). In hAD-Organs, recordings were performed at different culture stages (Fig. 7a,b). Among 167 recorded cells, 102 cells (60.1%) could generate action potentials. However, the ability to generate action potentials was dependent on reprogramming stages. We found that cells cultured for 100–140 days showed a higher probability of generating action potentials (65.2%, n = 135) than those cultured for a shorter period of time (80–100 days, 43.8%, n = 32). Among the cells with action potentials, 26.1% cells at 100–140 days and 7.1% cells at 80–100 days exhibited repetitive action potential firing (Fig. 7b). Spontaneous firing could also be detected occasionally (Extended Data Fig. 6a). In the 80–100-day group, the resting membrane potential (RMP) of cells that could generate action potentials was significantly more hyperpolarized than those without action potential generation (without action potential: −32.4 ± 3.8 mV, with action potential: −41.8 ± 1.7 mV; Extended Data Fig. 6b). For cells cultured for 100–140 days, no significant difference in RMP was detected between groups with and without action potentials (−34.7 ± 2.2 mV, −36.2 ± 1.1 mV; Extended Data Fig. 6b). However, among cells with action potentials, those with repetitive action potentials possessed a more hyperpolarized RMP (−41.3 ± 1.9 mV) than cells with a single action potential (−34.4 ± 1.3 mV; Extended Data Fig. 6c).

In addition, we examined the voltage-gated Na^+ currents at different culture stages (Fig. 7c,d). For cells cultured for less than 100 days, the peak amplitude of Na^+ currents was −247.5 ± 68.6 pA (Fig. 7d), significantly smaller than that of cells cultured for 100–140 days, which was −355.5 ± 25.8 pA (Fig. 7d). The application of 1 μM Tetrodotoxin (TTX) could completely block the Na^+ currents (n = 5; Fig. 7c). In cells cultured for 100–140 days, we also compared the peak amplitude of Na^+ currents between the single action potential group and the repetitive action potential group; no significant difference was detected (single action potential: −334.8 ± 28.4 pA, repetitive action potentials: −397.1 ± 52.6 pA; Extended Data Fig. 6d). We also occasionally observed spontaneous putative postsynaptic events (Extended Data Fig. 6e) at 100–140 days. Indeed, we observed the characteristic ultrastructure

https://doi.org/10.1038/s41551-022-00963-6

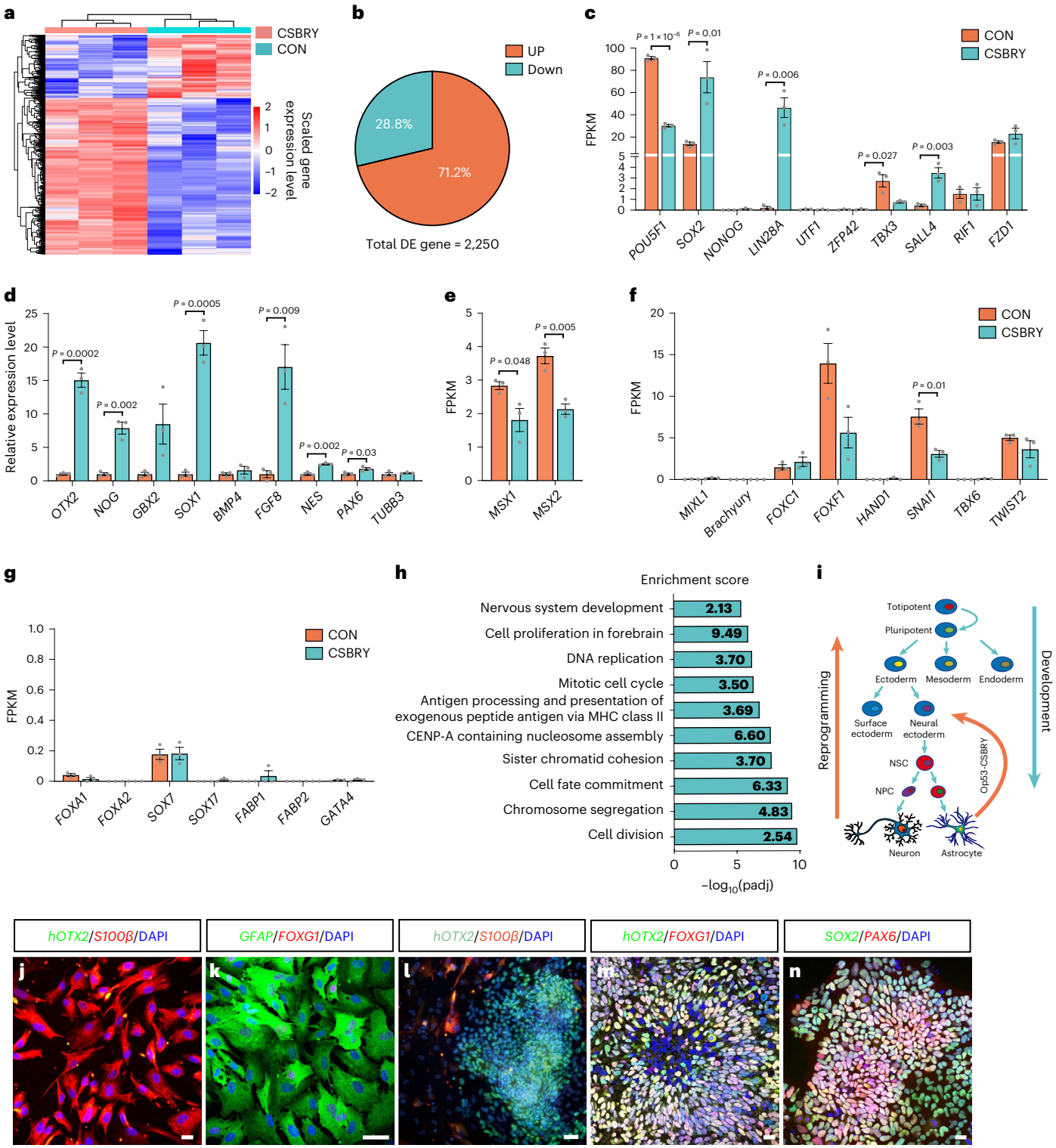

Fig. 6 | Visualization of the RNA sequencing dataset for transcriptional and subtype-specification analyses of the conversion of human astrocytes to neurons. a, Cluster analysis of differentially expressed genes comparing CSBRY with control treatment ($P < 0.05$, $\log_2FC > 1$). CON, control. **b**, Pie chart showing downregulated and upregulated genes in the CSBRY group compared with control (Op53/DMSO) treatment. **c**, Human embryonic stem cell marker gene expression profiles with CSBRY treatment ($n = 3$ independent experiments) of Op53/DMSO control. **d**–**g**, Graphs showing neural ectoderm (**d**), surface ectoderm (**e**), mesoderm (**f**) and endoderm (**g**) marker gene expression profiles with CSBRY treatment ($n = 3$ independent experiments) of Op53/DMSO control. **h**, Graph showing KEGG enrichment pathways of CSBRY treatment. padj, adjusted *P* value. **i**, Working model of Op53-CSBRY-induced astrocyte reprogramming. **j**–**n**, Representative images of the expression of the neural ectodermal marker *OTX2* (**j**) and forebrain marker *FOXG1* (**k**) in human primary astrocytes, and *OTX2* (**l**), *FOXG1* (**m**) and the neural epithelium cell marker *PAX6* and *SOX2* (**n**) expression in reprogrammed cells after CSBRY treatment at day 14. Scale bars, 50 μm. Data are presented as mean ± s.e.m. A multiple unpaired Student's *t*-test was used to compare each group. FPKM: fragments per kilobase per million, MHC: major histocompatibility complex, CENP-A: centromere protein A, Total DE gene: total differential expression gene.

https://doi.org/10.1038/s41551-022-00963-6

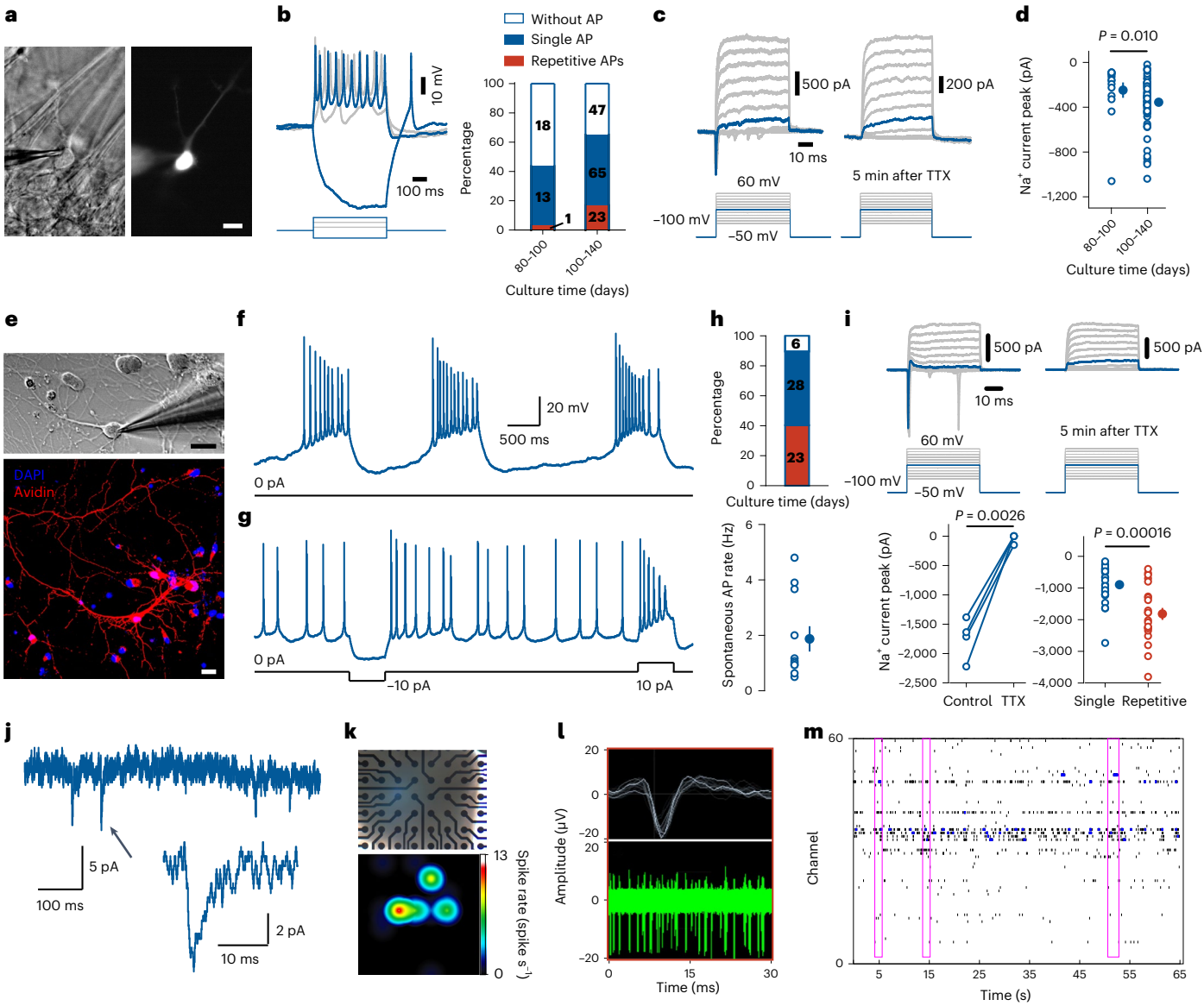

Fig. 7 | Electrophysiological characterization of hAD-Organs and hADSC-Organs. a, Infrared-differential interference contrast (left) and fluorescence (right) images of a recorded cell with action potentials (APs) ($n = 24$ cells). Scale bar, 10 μm. **b**, Left: membrane potential responses (top) to intracellular injections of step currents (bottom). The blue traces indicate the responses to +50/−30 pA current pulses. Note the rebound AP that occurred immediately after the negative pulse. Right: the percentage of AP generation for different culture times, and the number of recorded cells in each group. **c**, Example of whole-cell currents before (left) and 5 min after TTX application (right). The blue traces show the evoked currents when the membrane potential was stepped to 0 mV. **d**, Group data showing the peak amplitude of Na^+ currents with different culture times. Group 80–100 days: $n = 14$, group 100–140 days: $n = 69$. The Mann–Whitney test was used to compare the two groups. **e**, Infrared-differential interference contrast (top) and fluorescence (colour coded, bottom) images of a recorded cell with APs ($n = 23$ cells) from dissociated spinal-cord organoids. Scale bars, top: 20 μm, bottom: 50 μm. **f**, Spontaneous rhythmic bursting was detected in the cell shown in **e**. **g**, Spontaneous regular firing from another cell. The trace also shows responses to +10/−10 pA current pulses. **h**, Top: the percentage of cells without AP (white), with single AP (blue) and repetitive AP (red) at 7-week culture time. Bottom: spontaneous firing rate. **i**, Top: example of whole-cell currents before (left) and 5 min after TTX application (right). Bottom: group data showing the blockade of Na^+ currents by TTX (left) and the current amplitudes in cells with single and repetitive APs (right). Left: $n = 4$. An unpaired Student's t-test was used to compare with the control group. Right: single APs: $n = 26$, repetitive APs: $n = 22$. The Mann–Whitney test was used to compare single and repetitive APs. **j**, An example of trace showing spontaneous putative postsynaptic currents. A postsynaptic current event (arrow) was expanded for clarity (bottom right). **k**, Brightfield image of 8-week-old hADSC-Organs on a 64-electrode MEA plate (top), and an activity heatmap (bottom). **l**, Graphs showing neuron spikes that were detected by a single electrode in a 30-ms timeframe. **m**, Representative traces of the network activity of hADSC-Organs within a 65-s timeframe. Network bursts are labelled by pink boxes. Data are presented as mean ± s.e.m.

of synapses in 10-week-old hAD-Organs (Extended Data Fig. 6f), indicating that neurons in these organoids formed synaptic connections.

We examined spiking activities in cells from dissociated hADSC-Organs (7-week culture; Fig. 7e–m). Cells grew multiple neurites (Fig. 7e), and 89.5% (51/57) of the cells generated action potentials in response to step current injections (Fig. 7f–h). Among cells with action potentials, 45.1% (23/51) of the cells could fire repetitively, 27.5% (14/51) exhibited spontaneous firing and some of them showed rhythmic bursting (Fig. 7f). The averaged spontaneous firing rate was 1.9 ± 1.5 Hz (Fig. 7h). The RMP of cells that could generate action potentials was −33.4 ± 7.1 mV. Similarly, 1- μM TTX could completely block Na^+ currents ($n = 4$; Fig. 7i). In comparison with cells with a single action

potential (−896 ± 571 pA, $n = 26$), those with repetitive action potentials possessed much larger Na^+ currents (−1,818 ± 888 pA, $n = 22$; Fig. 7i). In some recorded cells, we again observed spontaneous putative post-synaptic events (Fig. 7j). In addition, to specifically record the action potential responses of motor neurons in hADSC-Organs, we labelled the neurons dissociated from hADSC-Organs with HB9::RFP lentivirus (LV). We found that 90% (18/20) of RFP^+ motor neurons (Extended Data Fig. 6g) could generate action potentials, and 38.9% (7/18) of them could fire repetitively (Extended Data Fig. 5h). Moreover, consistent with the above whole-cell recordings, recordings by a microelectrode array (MEA) also revealed spiking activities in whole hADSC-Organs (Fig. 7k,l) and showed neural network activities (Fig. 7m). Taken together, these results clearly showed that the neurons from both hAD-Organs and hADSC-Organs induced by Op53-CSBRY from human astrocytes were fully functional.

Characterization of hADSC-Organs grafted into a complete SCI in mice

Because hADSC-Organs had spinal-cord cellular characteristics, which included human ventral and dorsal spinal-cord progenitors, neuronal subtypes and cytoarchitectures, we explored whether hADSC-Organs supported spinal-cord regeneration in vivo after complete SCI. Acute transplantation may avoid growth inhibition and the formation of a glial scar to impede neural regeneration, which was found after SCI[2,3]. Thus, we immediately grafted 7-week-old hADSC-Organs labelled with *GFP* into the spinal cord of non-obese diabetic-severe combined immunodeficiency (NOD-SCID) mice that were completely resected 2–3 mm at T10. To enhance the regeneration capacity of hADSC-Organs, we combined hADSC-Organs with Matrigel to promote spatial integration with spared spinal-cord tissue, as well as the growth factors brain-derived neurotrophic factor (BDNF) and glial cell derived neurotrophic factor (GDNF) to support cell survival and growth (Fig. 8a). We found that hADSC-Organs highly expressed *GFP* after transduction by LV-Ubi-GFP virus (Extended Data Fig. 7a) and that they could grow up to about 2 mm, which is similar in size to a 1-month-old mouse spinal cord (Fig. 4c and Extended Data Fig. 7a,b). Furthermore, 7-week-old hADSC-Organs established their spinal-cord cellular identities, including both ventral and dorsal progenitors and major subtypes of neuron (Figs. 4i–l and 5a–f), indicating a cytoarchitecture comparable with spinal-cord tissue. After complete SCI, the mice showed hindlimb paralysis, suggesting a successful complete SCI model (Extended Data Fig. 7c and Supplementary Video 2). After 6-week transplantation, the hADSC-Organs survived and integrated with the spinal cords of the host mice (Fig. 8b and Extended Data Fig. 7d,e).

Next, we further characterized the subtypes of neuronal and glial cell in the graft region. Immunostaining results showed that the grafted hADSC-Organs expressed the neuronal markers *TUJ1* and *MAP2* but also included some $GFAP^+$ astrocytes (Fig. 8c–e). We observed inhibitory $GAD67^+$ and excitatory $VGLUT1^+$ mature neurons in the area of the transplanted spinal cord (Fig. 8f,g). Specifically, the hADSC-Organs contained motor neurons that maintained the characteristics of $ChAT^+$ spinal-cord motor neurons at 6 weeks after transplantation (Fig. 8h). These results indicated that hADSC-Organs maintained their spinal-cord cellular identities after in vivo transplantation. We further examined the integration and connectivity of grafted hADSC-Organs with host mice. We found that host spinal-cord neurons formed GFP^+/mouse anti-BSN^+ regenerated input synapses in the grafted hADSC-Organs region (Fig. 8i) and that human $synaptophysin^+$ synapses co-localized with $ChAT^+$ host spinal-cord motor neurons (Fig. 8j), demonstrating that synapses were formed between host neurons and the grafted hADSC-Organs. The grafted cells could migrate a long distance into the host ascending spared spinal cord, up to 2–3 mm from the lesion epicentre, and they sprouted neurites at the host spinal cord 6 weeks after transplantation (Fig. 8k). We also observed that $SMI312^+$ axons formed in the grafted hADSC-Organs, but no axons were newly generated in mice treated with Matrigel only (Extended Data Fig. 7g,h). Furthermore, we found that the grafted hADSC-Organs may reduce the size of the descending spared spinal cord (Fig. 8l–n), which may reflect the protective effects of the injured spinal cord. Together, these findings showed that grafted hADSC-Organs could survive, differentiate into spinal-cord neurons, re-establish synaptic connections with host neurons and bridge completely injured spinal-cord tissue in mice.

Behavioural analysis is an important indicator for evaluating the functional effects of organoid transplantation. Thus, we evaluated hindlimb locomotor movement after hADSC-Organ transplantation. We performed rigorous controlled experiments (four groups, 45 mice in total) and hADSC-Organ transplantation (25 mice) (Extended Data Fig. 7f). Unfortunately, we found no detectable improvement in spontaneous locomotor functions after hADSC-Organ transplantation at week 6 (Extended Data Fig. 7f and Supplementary Table 1). However, a few mice grafted with hADSC-Organs showed hindlimb locomotor responses after strong stimulation (Supplementary Video 3), which suggested that spinal-cord organoid transplantation has the potential to enhance locomotor functions after complete SCI. In summary, our studies showed that grafted hADSC-Organs could maintain their spinal-cord cellular identities, integrate with mouse host neurons and that they may help bridge the complete SCI.

Discussion

Previous studies have reported that human astrocytes can be reprogrammed into different types of postmitotic neuron[29,30,33,34,36,37,47], but whether 3D brain-region-specific organoids can be directly generated from human primary astrocytes has remained unclear. In this study, we first established a virus-free and integration-free chemically defined system to directly convert human astrocytes into neural ectodermal cells, which directly formed 3D cortical organoids and were guided into spinal-cord organoids that possessed the developing spinal-cord identities with dorsoventral and rostrocaudal spatial cytoarchitectures. The grafted hADSC-Organs survived, differentiated into spinal-cord neurons, migrated long distances, formed synaptic connectivity with host neurons and might bridge the complete SCI. This study shows the potential of endogenous astrocyte reprogramming for neural organogenesis of the CNS after injury.

Direct cellular reprogramming for tissue regeneration has been attempted[25,27,48], with the potential to reduce immune rejection. Direct somatic cell reprogramming has the potential for in situ organogenesis within damaged organs[28,36]. Tissue loss in the central neural system is irreversible after injury. Thus far, in situ neural organogenesis remains a challenge[49]. Previous studies have shown that resident astrocytes can be directly reprogrammed into neurons via the ectopic expression of transcription factors, microRNA or small molecules[26,28–35,47]. However, the methods of chemical reprogramming have shown that human astrocytes bypass a proliferative state and directly convert into postmitotic neurons, which have no ability for proliferation and neural organogenesis[30,34]. Moreover, the conversion efficiency was low. To improve on this, we found that the CSBRY cocktail robustly enhanced human astrocyte reprogramming by about 240-fold. Critically, Op53-CSBRY-reprogrammed cells specifically obtained a neural ectodermal state, which had the ability to rapidly proliferate and spontaneously form cortical organoids. They could then be patterned into spinal-cord organoids via ventralizing and dorsalizing morphogens. Previous studies have shown that mature astrocytes could be directly converted into NSCs by *OCT4* in rats, which was enhanced by SHH[50]. Another study reported that six small molecules, including A83-01, CHIR99021, sodium butyrate, lysophosphatidic acid (LPA), rolipram and SP600125, combined with the overexpression of *OCT4*, could convert human neonatal fibroblast cells into hNSCs that also expressed *PAX6* and *OTX2*[51]. Here we showed that the four-compound cocktail CSBRY combined with *OCT4* and the knockdown of *p53* can directly reprogramme human astrocytes into neural ectodermal cells, which

https://doi.org/10.1038/s41551-022-00963-6

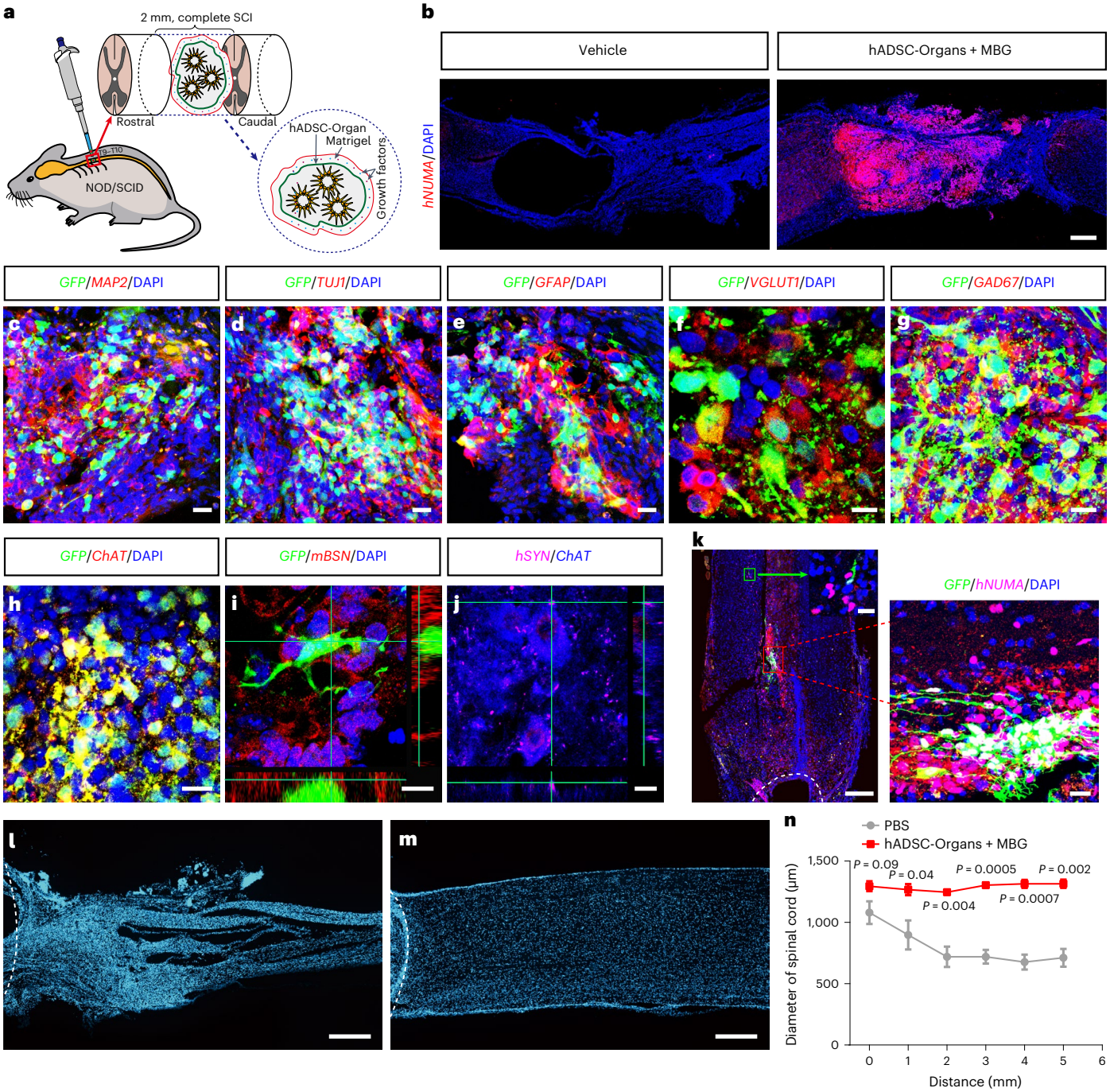

Fig. 8 | In vivo survival and neural connectivity of hADSC-Organs transplanted into a complete SCI in mice. a, Schematic illustrating the experimental study. At week 7, hADSC-Organs labelled with *GFP* were grafted immediately into a T9–T10 spinal cord after complete section in immunodeficient NOD-SCID mice. **b**, Images of vehicle control (left) and grafted hADSC-Organs integrated at the lesion epicentre (right). Scale bars, 250 μm. **c**,**d**, Immunostaining showing the neuronal morphology of hADSC-Organs at week 6 after transplantation into a mouse's spinal cord, using the neuronal markers *MAP2* (**c**) and *TUJ1* (**d**). Scale bars, 25 μm. **e**–**h**, Immunostaining showing that transplanted hADSC-Organs after 6 weeks could differentiate into GFAP$^+$ (**e**) astrocytes and the VGLUT1$^+$ (**f**), GAD67$^+$ (**g**) and ChAT$^+$ (**h**) subtypes of mature neuron. Scale bars, 25 μm (**e**,**g**–**h**) and 10 μm (**f**). **i**, The host-specific presynaptic marker *Bassoon* (*BSN*) was co-localized with *GFP*-positive grafted neurons at the section of transplanted hADSC-Organs after 6 weeks. Scale bar, 10 μm. **j**, The human-specific presynaptic marker *hSyn* co-localized with host ChAT$^+$ neurons. Scale bar, 10 μm. Immunofluorescence images were captured at serial optical sections, one xy optical section and reconstructed xz (bottom edge) and yz (right edge) images of the regions showing the co-localization sites of labeled markers (the intersection of green lines) are shown in **i** and **j**. **k**, hNUMA$^+$/GFP$^+$-transplanted cells migrated long distances into the host's spinal cord. Dotted white lines outline the region where the hADSC-Organs were implanted. Scale bar, 250 μm. The expanded green box and the expanded red box show zoomed-in images. Scale bars, 20 μm. **l**,**m**, Representative images of a spinal cord implanted with vehicle control (left) and hADSC-Organs + MBG (right). Scale bars, 500 μm. MBG, Matrigel + BDNF + GDNF. **n**, Quantitative analysis of the size of the dystrophy of the descending spared spinal cord for the vehicle control and hADSC-Organs + MBG at each distance from the lesion ($n = 3$ mice). Data are presented as mean ± s.e.m. Representative images are from the section of the spinal cord ($n = 3$ mice). Multiple unpaired Student's *t*-tests were used for comparisons.

can be directly guided into brain-region-specific organoids, displaying a high capability for organogenesis. Our findings may indicate that local astrocytes have the potential for in situ organogenesis after brain damage from stroke or SCI, for example.

SCI, especially complete SCI, leads to the loss of spinal-cord tissue, including extensive neural cell and neural fibre loss. Research into spinal-cord neural regeneration has often shown conflicting or controversial results[3,12]. The main strategies for restoring extensively lost spinal-cord neural cells are reactivating neurogenesis using endogenous neural cells or cell replacement via the transplantation of exogenous cells. Recent studies have shown that a graft of hPSC-derived spinal-cord NSCs helped axonal regeneration, promoted functional recovery after SCI in mice[9] and also showed restorative effects after transplantation into the primate spinal cord[52]. Previous studies have reported that transplanting hiPSC-derived neurospheres induced synapse formation with host neurons, promoted axonal growth and led to significant functional recovery in contusion spinal-cord mice[11]. Here we report that human endogenous astrocytes can be directly reprogrammed into hADSC-Organs in vitro that have developing spinal-cord cellular identities and show similar cytoarchitecture to the spinal cord. The grafted hADSC-Organs survived, differentiated into the major spinal-cord neural cells, formed synapses with host neurons and bridged the host's injured spinal-cord tissue. However, we found no detectable improvement in spontaneous locomotor functions 6 weeks after transplantation; only some of the hADSC-Organs-treated mice showed locomotor responses after stimulation (Supplementary Video 3). One reason is that the grafted cells and host tissue are from different species and thus may not form effective functional synapses. Another reason is that the hADSC-Organs do not have the in vivo architecture of the human spinal cord (for instance, dorsal and ventral neuronal nuclei or white matter structures), which may better facilitate the connection with murine spinal-cord tissue. Thus, our induction method for hADSC-Organs could benefit from optimization, for example by using engineered biomaterials to mimic damaged spinal-cord tissue, for improved functional outcomes.

In summary, we established a genetic-integration-free and chemically defined method to directly generate cortical and spinal-cord organoids from human astrocytes through early neuroectodermal cells. Furthermore, we confirmed that when these hADSC-Organs were grafted into a complete SCI, they could survive, maintain their spinal-cord cellular characteristics, form synaptic connectivity with host neurons and bridge the injured spinal-cord tissue. Our findings suggest that neural organoid therapy may be a promising strategy for neural organogenesis. If combined with a biomaterial delivery system, the direct reprogramming of human astrocytes could allow in situ organogenesis. Future studies could optimize the organoid-induced spinal-cord conditions and examine whether the Op53-CSBRY protocol can directly reprogram astrocytes in situ into a spinal-cord organ in a non-human-primate SCI model.

Methods

Human astrocyte culture

Commercially acquired primary astrocytes isolated from the human brain cerebral cortex (catalogue no. 1800, Sciencell) were cultured in Matrigel (catalogue no. 365230, BD)-coated plates using the astrocyte medium (AM) (catalogue no. 1801, Sciencell). The medium was changed every other day. Cells were passaged with TrypLE (Thermo Fisher Scientific) and neutralized with DMEM (Thermo Fisher Scientific) with 10% fetal bovine serum (FBS) (Thermo Fisher Scientific), and they were used for this study at passages 4–8. These human primary astrocytes were used in all the reprogramming experiments excluding those in Fig. 2c–f.

hESCs (H9, WiCell) were maintained in Matrigel-coated plates with E8 medium (Gibco). For astrocyte differentiation, H9 cells were cultured in low attachment flasks in the serum replacement medium (SRM) medium (DMEM, 15% knockout serum replacement, 2 mM L-glutamine and 10 μM β-mercaptoethanol) and treated with LDN193189 (100 nM, Stemolecule) and SB431542 (10 μM, MedChemExpress) from day 0 to day 7. Spheres were grown in the N2aa medium (DMEM-F12 with 1% N_2 and 200 μM L-ascorbic acid) and supplemented with 20 ng ml^{-1} of bFGF and 20 ng ml^{-1} of EGF from day 8 to day 14. From day 15, spheres were dissociated into single cells and reseeded in a Matrigel-coated plate with AM and passaged every 3–5 days.

Human mature astrocytes were dissociated from the tissue of patients (aged between 13 and 65 years) with gliomas sided to the focal lesion tissue. The samples were cut into 1-mm blocks and digested with papain for 1 h at 37 °C. They were then neutralized with DMEM + 10% FBS and cultured in a Matrigel-coated plate with AM. The protocol for collecting astrocytes was permitted by the scientific research sub-committee of the medical ethics committee of Zhongshan Hospital affiliated with Xiamen University.

Human astrocyte reprogramming and small-molecule screening

Human astrocytes were cultured in 6-cm or 10-cm plates until 90% confluence, and 5–6 μg of pCXLE-hOCT3/4-shp53-F (Addgene No. 27077) plasmid mixtures were electroporated into ~1 × 10^6 cells using the program T-020 (Lonza) with a 100-μl reagent kit (Lonza, VPD1001) according to the manufacturer's instructions. On day 0, the cells were seeded onto 2 × 10^4 cells well^{-1} in a 24-well plate coated with Matrigel. The next day, the culture medium was replaced with fresh AM. After 3 days of transduction, the cells were switched to the neural medium including the neurobasal medium (Thermo Fisher Scientific), glutmax (1:100, Thermo Fisher Scientific), Non-Essential Amino Acids (1:100, Thermo Fisher Scientific), 2% B27 supplements (Thermo Fisher Scientific), 20 ng ml^{-1} of BDNF (Peprotech), 20 ng ml^{-1} of GDNF (Peprotech), 200 μM L-ascorbic acid 2-phosphate (Sigma) and 100 U ml^{-1} of penicillin and streptomycin (Thermo Fisher Scientific). From day 3 to day 8, small molecules including CHIR99021 (1.5 μM, Tocris), valproic acid (5 mM, Cayman), RepSox (1 μM, Tocris), forskolin (10 μM, Cayman), JQ1 (50 nM, Sigma), ISX-9 (10 μM, Tocris), LDN193189 (100 nM, Stemolecule), TTNPB (0.5 μM, Tocris), Y27632 (10 μM, Tocris), DAPT (2.5 μM, Sigma), SAG (100 nM, EMD Millipore), SB431542 (10 μM, MedChemExpress), PD0325901 (10 μM, Tocris), SU5402 (10 μM, Biovision) and XAV939 (10 μM, Tocris) were added to induce neurons cultured with the neural medium for primary screening. CHIR99021, SB431542, RepSox and Y27632 were selected as the different combinations for second screening. The cells were treated by these small molecules for 5 days. At day 8, the drugs were removed, and the cells were changed into fresh neural medium. The medium was changed every 2–3 days. On day 21, cells were fixed for neuronal marker *MAP2* immunostaining.

Generation of cortical organoids from human astrocytes

For the generation of cortical organoids, on day 0, human astrocytes electroporated with pCXLE-hOCT3/4-shp53-F were seeded 2 × 10^5 cells well^{-1} into a six-well plate coated with Matrigel. The next day, the culture medium was replaced with fresh AM. From day 3 to day 8, the cells were treated with CSBRY in the neural medium. From day 9 to day 13, the induced astrocytes were expanded in the neural medium. On day 14, the induced astrocytes were transferred to ultralow-attachment 24-well plates (Corning) with 2–3 × 10^5 cells well^{-1} for suspension culture when large amounts of neural precursors appeared. The ROCK inhibitor Y27632 (10 μM) was added to promote the survival of cells on the first day of reseeding. From day 15, the neural spheroids were generated in each well in 24-well plates on an orbital shaker and then continually maintained in the neural medium, which was changed every 2–3 days. At day 21, spheroids were embedded with Matrigel. The spheroids were then transferred into an ultralow-attachment 60-mm dish on an orbital shaker for long-term culture.

Generation of spinal-cord organoids from human astrocytes

For the generation of spinal-cord organoids, from day 0 to day 14, the protocol was the same as the induced cortical organoids. From day 15 to day 18, the spheroids were induced with bFGF (20 ng ml^{-1}, Peprotech) and retinoic acid (100 nM, Sigma) in the neural medium. On day 18, bFGF and retinoic acid were replaced with the SHH signalling agonist SAG (500 nM) lasting for 10 days. Next, from day 28 to day 31, the spheroids were treated with BMP4 (15 ng ml^{-1}, Peprotech), and the previous drug was withdrawn. During this course, spheroids were embedded with Matrigel and then transferred into an ultralow-attachment 60-mm dish on an orbital shaker on day 21 for long-term culture, with the medium exchanged every 2–3 days. After 7 weeks, the spheroids were collected for further analysis.

For transplantation of spinal-cord organoids, the induced cells were infected with the LV-Ubi-GFP virus at day 13 before reseeding to an ultralow-attachment 24-well plate. The other induced procedures were the same as described above.

Immunofluorescence staining

For immunocytochemistry, cells were fixed for 20 min at room temperature in 4% paraformaldehyde (PFA) in phosphate-buffered saline (PBS), washed three times with PBS for 10 min each, then blocked for 20 min in PBS containing 3% bovine serum albumin (BSA) and 0.3% Triton X-100 and washed three times with PBS for 10 min. Fixed cells were incubated overnight at 4 °C with the primary antibodies (Supplementary Table 2) in PBS with 3% BSA. The cells were then washed three times with PBS for 10 min each and incubated with secondary antibodies in PBS with 1% BSA for 1 h at room temperature. The cell nuclei were stained with DAPI.

Cortical organoids and spinal-cord organoids were fixed in 4% PFA overnight at 4 °C and then transferred to 30% sucrose. After sinking to the bottom, organoids were embedded in the optimum cutting temperature embedding medium and sectioned in a cryostat with 20-μm-thick slices. Serial sections of organoids were attached to slide glasses. Following air drying at 37 °C, the sample slices were permeabilized and blocked in PBS with 3% BSA and 0.3% Triton X-100 for 20 min at room temperature and incubated with primary antibodies at 4 °C overnight. Next, the slices were washed three times in PBS and incubated with secondary antibodies (Alexa Fluor 488-, 594- and 638-conjugated antibodies, 1:500) for 1 h at room temperature. Cultured slices from dissociated hADSC-Organs were performed with a similar protocol, instead incubated with streptavidin (1:1,000, Thermo Fisher Scientific, S11227). The nuclei were stained with DAPI.

Western blotting

Protein samples were collected on day 3 after the transduction of plasmids. Proteins (30 μg) were separated on 12% SDS–PAGE and transferred to a polyvinylidene difluoride (PVDF) membrane. The membranes were incubated at 4 °C overnight with the primary antibodies: OCT3/4 (mouse, 1:1,000, BD Bioscience, 561555), p53 (rabbit, 1:300, Epitomics, 1026-1) and GAPDH (rabbit, 1:5,000, Abcam, ab181602). Horseradish peroxidase-conjugated anti-mouse or anti-rabbit IgG was used as a secondary antibody. Chemiluminescence (Yeasen, Super ECL Detection Reagent, 36208ES60) was used to develop the signals.

Electrophysiological recordings and analysis

Culture slices prepared for whole-cell recording were transferred to an incubation chamber and perfused with artificial cerebrospinal fluid (ACSF). Whole-cell recordings were performed using patch pipettes with an impedance of 4–7 MΩ. The temperature was maintained at 34.5–35.5 °C. An infrared-differential interference contrast microscope (BX-51WI, Olympus) was used for the visualization of culture cells. A multiclamp 700B amplifier (Molecular Devices) and a Power1401-3A analogue-to-digital converter were used for data acquisition. Spike2 version 10 and Signal software version 8 (Cambridge Electronic Design) together with MATLAB (MATHWORKS R2021a) were used for data analysis. The ACSF contained 126 mM NaCl, 2.5 mM KCl, 26 mM $NaHCO_3$, 1.25 mM NaH_2PO4, 2 mM $MgSO_4$, 2 mM $CaCl_2$ and 25 mM dextrose (315 mOsm, pH 7.4) and was bubbled with 95% O_2 and 5% CO_2. The pipette solution contained 130 mM K-gluconate, 10 mM KCl, 4 mM MgATP, 0.3 mM Na_2GTP, 10 mM HEPES, 10 mM Na_2-phosphocreatine and 0.2% biocytin (288 mOsm, pH 7.29) or 140 mM K-gluconate, 3 mM KCl, 2 mM $MgCl_2$, 10 mM HEPES, 0.2 mM EGTA, 2 mM Na_2ATP and 0.2% biocytin (285–295 mOsm, pH 7.2). In some recordings, Alexa Fluor 488 dye (Invitrogen) was loaded to show cell morphology.

To induce AP initiation in the culture cells, positive current pulses (10 pA $step^{-1}$, 500 ms in duration) were injected to examine the electrophysiological properties when the cell was at the RMP. To obtain the Na^+ currents, cells were held at −100 mV for 80 ms and then depolarized to different membrane potential levels (from −90 to 60 mV, 10 mV $step^{-1}$) for 50 ms. P/N subtractions were performed offline by using Signal software. Na^+ current amplitudes were further analysed using MATLAB (MATHWORKS). The spontaneous firing rate was measured from a 30-s stable recording. The liquid junction potential (15–16 mV) was not corrected for the membrane potential shown in the text and figures. For group comparison, the Shapiro–Wilk test was used for the data normality test. A two-sample Student's *t*-test was used if they were normally distributed; otherwise, the Mann–Whitney *U* test was employed. Data were presented as mean ± s.e.m. in the text and figures.

MEA recording for hADSC-Organs

MEA was used to detect the neuronal spike. Each well of six-well MEA plates (Axion Biosystems) contains 64 low-impedance platinum microelectrodes (0.04 MΩ $microelectrode^{-1}$) with a diameter of 30 mm, which are spaced 200 mm apart. The plate was pre-coated with Matrigel 1:100 diluted in the DMEM medium at an incubator for 30 min. One 9-week-old spinal-cord organoid was placed into a coated MEA well to cover 64 microelectrodes. Matrigel was added to immobilize the spinal-cord organoid at the incubator for 10 min, and then fresh neural medium was added. Recordings for 10–15 min were performed using a Maestro pro MEA system and AxIS Software Spontaneous Neural Configuration (Axion Integrated Studio Navigator 1.5, Axion Biosystems).

For data analysis, the Neural Metric Tool (Axion Biosystems) was used to classify active electrodes that detected at least 5 spikes min^{-1}. Spike bursts were then identified on the basis of an interspike interval threshold requiring a minimum number of five spikes with a maximum interspike interval of 100 ms.

Virus package

The 293T cells were plated to collagen I (5 μg cm^{-2})-coated 10-cm dishes with 3×10^6 cells and cultured for 24 h in 10 ml of DMEM medium with 10% FBS, 4 mM L-glutamine, 100 U ml^{-1} penicillin and streptomycin and 0.1 mM MEM NEAA. After 24 h, the medium was replaced 1–3 h before transfection with 8 ml of pre-warmed fresh DMEM medium. For each 10-cm dish, 20 μg of total plasmid DNA (10 μg of LV-Ubi-GFP or LV-HB9::RFP and 7.2 μg of PSPAX2 and 6.8 μg of MD2G) was diluted in 0.5 ml of 0.25 M calcium chloride solution. The diluted plasmid DNA was mixed gently with an equal volume of 0.5 ml of 2× Hanks balanced salt solutions (HBS) (pH 7.05) and immediately added into the dish drop by drop, and then the cells were incubated at 37 °C in 5% CO_2 after swirling the plate. Next, the supernatant was collected in a 50 ml tube at 24, 48 and 72 h after transfection, followed by centrifugation of the supernatant at 3000 r.p.m. at 4 °C for 10–15 min. Finally, aliquots of 100 μl of supernatant were stored at −80 °C.

FACS analysis

Cells were isolated using TrypLE and fixed with 4% PFA for 15 min, washed three times with PBS and then resuspended in PBS buffer containing 2% normal serum (FACS buffer). The primary antibody MAP2 (1:500) was then added to each sample and incubated on ice for 1 h.

Next, the secondary conjugated antibody was added to each sample and incubated on ice for 30–60 min. The cells were then washed three times with PBS, resuspended in FACS buffer and analysed on a Beckman Gallios flow cytometer. Data analysis was performed using FlowJo software version 10.62.

Time-lapse imaging

Human astrocytes were electroporated with the pCXLE-hOCT3/4-shp53-F plasmid and then cultured in a Matrigel-coated 35-mm dish. After treated with CSBRY for 5 days, the cells were infected with 10 µl of ssAAV-pGFAP-EGFP-WPREs virus suspension for 6–8 h. For live cell tracing, GFP-positive cells were imaged using a epifluorescent microscope (Zesi TE-2000-S) for 4 days with snapshots every half an hour. After time-lapse imaging, the cells were fixed and MAP2 immunostaining was performed.

Electron microscopy

Ten-week-old organoids were immersed in a fixative (2.5% glutaraldehyde in 0.1 M PBS buffer, pH 7.4) at 4 °C for at least 4 h, washed three times with 0.1 M PBS buffer at 4 °C for 1 h, postfixed in 1% osmium tetroxide in 0.15 M cacodylate buffer at 4 °C for 2 h and stained in 2% uranyl acetate for 1 h. Organoids were dehydrated in an ethanol gradient (30%, 50%, 70%, 90% and 100% ethanol), embedded in Spur's resin. Samples were sectioned at 60 nm on a Leica Ultracut UCT (Leica, Bannockburn, IL), transferred onto copper grids and stained with 2% uranyl acetate for 5 min and lead citrate stain for 1 min. Grids were analysed using an HT-7800 transmission electron microscope (Hitachi).

Thoracic complete section surgery and transplantation

Adult male NOD-SCID mice (20–22 g) were anaesthetised and maintained with 0.8% isoflurane throughout the surgical procedure. By performing laminectomy, we exposed the dorsal portion of the spinal cord (T9–T10 levels). The dorsal and ventral complete section with a length of 2–3 mm at the T10 level was removed with spring scissors. GFP-labelled spinal-cord organoids with Matrigel including BDNF (20 ng ml^{-1}) and GDNF (20 ng ml^{-1}) were transplanted into the lesion region using a cut pipette after the complete section. An equal volume of PBS or Matrigel was injected into mice as a control. The cover muscles and skin at the site of injury were sutured with stylolite. Bladders of damaged animals were squeezed daily to help the mice urinate during the experimental course. All experimental protocols were approved by the Institutional Animal Care and Use Committee at Xiamen University and complied with all relevant animal-use guidelines and ethical regulations.

Behavioural and histological analyses

Behavioural analyses were evaluated by two observers with a double-blind approach according to the criteria for the Basso–Beattie–Bresnahan score. For immunohistochemistry, after 6 weeks of transplantation, mice were deeply anesthetized and cardiacally perfused with first PBS and then 4% PFA (pH 7.4). The dissected spinal cords were fixed in 4% PFA at 4 °C overnight and dehydrated with 30% sucrose at 4 °C for 1 day. Using a cryostat, we then cut the dehydrated tissue into axial sections. Following air drying at 37 °C, the sections were permeabilized and blocked in PBS with 3% BSA and 0.3% Triton X-100 for 20 min at room temperature and incubated with primary and secondary antibodies according to the normal immunostaining protocol.

RNA sequencing

For RNA sequencing, three biological repeats were used including CSBRY treatments and control groups and hAD-Organs compared with hADSC-Organs. Total RNA was extracted using RNAiso Plus (Takara, 9109) according to the manufacturer's protocol. RNA purity and quantification were evaluated using a NanoDrop 2000 spectrophotometer (Thermo Scientific). RNA integrity was assessed using an Agilent 2100 Bioanalyzer (Agilent Technologies). The libraries were then constructed using the TruSeq Stranded mRNA LT Sample Prep Kit (Illumina) according to the manufacturer's instructions. The transcriptome sequencing and analysis were conducted by OE Biotech Co., Ltd. The libraries were sequenced on an Illumina HiSeq X Ten system and 150-bp paired-end reads were generated. Raw data (raw reads) of the fastq format were first processed using Trimmomatic version 0.36, and about 40–65 millions (M) raw reads for each sample were generated. Then about 40–65 M clean reads for each sample remained, which were obtained for downstream analyses by removing reads containing adapter, reads containing ploy-N and low-quality reads from raw data. The clean reads were mapped to the human genome using HISAT2 version 0.36. The FPKM value of each gene was calculated using Cufflinks version 2.2.1, and the read counts of each gene were obtained by HTSeq-count. Differential expression analysis was performed using the DESeq (2012) R package. A P value of <0.05 and a fold change of >2 or <0.5 were set as the threshold for significantly differential expression. Hierarchical cluster analysis of differentially expressed genes was performed to explore gene expression patterns. Gene ontology enrichment and KEGG pathway enrichment analysis of differentially expressed genes were performed using R version 3.6.1 on the basis of the hypergeometric distribution.

Single-cell RNA sequencing

To characterize the cell subtype population of primary human astrocytes (HA1800) and hADSC-Organs, single-cell RNA sequencing was performed using 10x Genomics. To identify human astrocyte subtypes, the cultured astrocytes were dissociated into single-cell suspensions using TrypLE. For hADSC-Organ population analysis, four hADSC-Organs were transferred into fresh neural medium and cut into small pieces. The hADSC-Organ pieces were dissociated into single cells by incubating in a papain-based solution containing papain (20 U ml^{-1}, LS03126, Worthington), DNase I (10 µg ml^{-1}, 11284932001, Sigma) and L-cysteine hydrochloride monochloride (180 µg ml^{-1}, C7880, Sigma) at 37 °C for 15 min. The organoid pieces were then triturated using 1-ml tips at incubation intervals of 5–10 min, amounting to about 45 min of incubation. The dissociated cells were then centrifuged at 500 g for 5 min, resuspended in the neurobasal medium containing 10% FBS and filtered using a 30-µm cell strainer. After measuring the density and viability of astrocytes or hADSC-Organ-dissociated cells, the final cell density was modified into 300–600 cells $µl^{-1}$. Dissociated single cells mixed with enzymes and the beads containing barcode information were wrapped by oil droplets and loaded onto a Chromium Single Cell 3′ Chip to form gel bead-in emulsions. cDNA products were obtained after cell lysis and reverse transcription reaction in gel bead-in emulsions, which were then connected with a barcode. Subsequently, gel bead-in emulsions were broken followed by PCR amplification of cDNA templates. Agilent 4200 was used for the qualification of amplification products, and single-cell RNA sequencing libraries were prepared with the 10x Genomics Chromium Single Cell 3′ Library and Gel Bead Kit v3. Then, via Illumina NovaSeq6000, sequencing was performed to obtain 150-bp paired-end reads. Obtained reads were aligned to the human reference genome (GRCh38) using Cell Ranger version 3.0. Then, filtering barcode and unique molecular identifier (UMI) counting were conducted. After counting reads for each feature in each cell, the R package Seurat version 4.0 was applied for further analysis.

Genes that were not expressed in at least ten cells and cells expressed with more than 6,000 and less than 1,000 detected genes were excluded, as well as those with mitochondrial content more than 10%. Gene expression of cells was normalized using a global-scaling normalization method (normalization method = 'LogNormalize') and scaled using R package Seurat (scale factor = 10,000). To perform the principal component analysis, the top 1,500 high variable genes were selected and scaled. The top 20 principal components were utilized to construct the nearest-neighbour graph using FindNeighbors, and cell

clusters were identified by the function FindClusters with a resolution of 0.8 in Seurat. Finally, we classified cell clusters of human astrocyte and hADSC-Organs on the basis of the expression of known markers of astrocytes or spinal cord[5,45,46].

Statistical analysis and reproducibility

Data are presented as mean ± s.e.m. The unpaired two-tailed *t*-test, Mann–Whitney *t*-test and ordinary one-way ANOVA using GraphPad Prism software version 7.0 were used to determine the statistical significance. The significance levels are $^{*}P < 0.05$, $^{**}P < 0.01$ and $^{***}P < 0.001$. All the statistical tests and biological replicates are explained in the figure legends. Direct reprogramming of human astrocytes by Op53-CSBRY is reproducible with over 25 independent experiments and generated about 50 cortical organoids and 80 spinal-cord organoids in this study.

Reporting summary

Further information on research design is available in the Nature Portfolio Reporting Summary linked to this article.

Data availability

The data supporting the results in this study are available within the Article and its Supplementary Information. The RNA sequencing data are available from the Gene Expression Omnibus database via the accession number GSE168635. The raw single-cell RNA sequencing data are available from the Genome Sequence Archive database via the accession number https://ngdc.cncb.ac.cn/gsa-human/browse/HRA002541. Source data are provided with this paper.

References

1. Anderson, M. A. et al. Required growth facilitators propel axon regeneration across complete spinal cord injury. *Nature* **561**, 396–400 (2018).
2. Courtine, G. & Sofroniew, M. V. Spinal cord repair: advances in biology and technology. *Nat. Med.* **25**, 898–908 (2019).
3. Sofroniew, M. V. Dissecting spinal cord regeneration. *Nature* **557**, 343–350 (2018).
4. Li, K. et al. Human iPS cell-derived astrocyte transplants preserve respiratory function after spinal cord injury. *Exp. Neurol.* **271**, 479–492 (2015).
5. Andersen, J. et al. Generation of functional human 3D cortico-motor assembloids. *Cell* **183**, 1913–1929 (2020).
6. Lu, P. et al. Prolonged human neural stem cell maturation supports recovery in injured rodent CNS. *J. Clin. Invest.* **127**, 3293–3305 (2017).
7. Kawai, M. et al. Long-term selective stimulation of transplanted neural stem/progenitor cells for spinal cord injury improves locomotor function. *Cell Rep.* **37**, 110019 (2021).
8. Fischer, I., Dulin, J. N. & Lane, M. A. Transplanting neural progenitor cells to restore connectivity after spinal cord injury. *Nat. Rev. Neurosci.* **21**, 366–383 (2020).
9. Kumamaru, H. et al. Generation and post-injury integration of human spinal cord neural stem cells. *Nat. Methods* **15**, 723–731 (2018).
10. Lu, P. et al. Long-distance axonal growth from human induced pluripotent stem cells after spinal cord injury. *Neuron* **83**, 789–796 (2014).
11. Nori, S. et al. Grafted human-induced pluripotent stem-cell-derived neurospheres promote motor functional recovery after spinal cord injury in mice. *Proc. Natl Acad. Sci. USA* **108**, 16825–16830 (2011).
12. Assinck, P., Duncan, G. J., Hilton, B. J., Plemel, J. R. & Tetzlaff, W. Cell transplantation therapy for spinal cord injury. *Nat. Neurosci.* **20**, 637–647 (2017).
13. Marchini, A. et al. Multifunctionalized hydrogels foster hNSC maturation in 3D cultures and neural regeneration in spinal cord injuries. *Proc. Natl Acad. Sci. USA* **116**, 7483–7492 (2019).
14. Lai, B. Q. et al. A modular assembly of spinal cord-like tissue allows targeted tissue repair in the transected spinal cord. *Adv. Sci.* **5**, 1800261 (2018).
15. Ogura, T., Sakaguchi, H., Miyamoto, S. & Takahashi, J. Three-dimensional induction of dorsal, intermediate and ventral spinal cord tissues from human pluripotent stem cells. *Development* **145**, dev162214 (2018).
16. Koffler, J. et al. Biomimetic 3D-printed scaffolds for spinal cord injury repair. *Nat. Med.* **25**, 263–269 (2019).
17. Di Lullo, E. & Kriegstein, A. R. The use of brain organoids to investigate neural development and disease. *Nat. Rev. Neurosci.* **18**, 573–584 (2017).
18. Pasca, S. P. The rise of three-dimensional human brain cultures. *Nature* **553**, 437–445 (2018).
19. Lancaster, M. A. et al. Cerebral organoids model human brain development and microcephaly. *Nature* **501**, 373–379 (2013).
20. Park, S. E., Georgescu, A. & Huh, D. Organoids-on-a-chip. *Science* **364**, 960–965 (2019).
21. Qian, X. Y. et al. Brain-region-specific organoids using mini-bioreactors for modeling ZIKV exposure. *Cell* **165**, 1238–1254 (2016).
22. Cakir, B. et al. Engineering of human brain organoids with a functional vascular-like system. *Nat. Methods* **16**, 1169–1175 (2019).
23. Pasca, A. M. et al. Human 3D cellular model of hypoxic brain injury of prematurity. *Nat. Med.* **25**, 784–791 (2019).
24. Trujillo, C. A. et al. Complex oscillatory waves emerging from cortical organoids model early human brain network development. *Cell Stem Cell* **25**, 558–569 (2019).
25. Li, H. D. & Chen, G. In vivo reprogramming for CNS repair: regenerating neurons from endogenous glial cells. *Neuron* **91**, 728–738 (2016).
26. Niu, W. Z. et al. In vivo reprogramming of astrocytes to neuroblasts in the adult brain. *Nat. Cell Biol.* **15**, 1164–1194 (2013).
27. Srivastava, D. & DeWitt, N. In vivo cellular reprogramming: the next generation. *Cell* **166**, 1386–1396 (2016).
28. Zheng, Y. Y. et al. In vivo reprogramming of reactive astrocytes into functional neurons after cervical spinal cord injury. *J. Neurotrauma* **35**, 180–181 (2018).
29. Cervo, P. R. D. et al. Induction of functional dopamine neurons from human astrocytes in vitro and mouse astrocytes in a Parkinson's disease model. *Nat. Biotechnol.* **35**, 444–452 (2017).
30. Gao, L. F. et al. Direct generation of human neuronal cells from adult astrocytes by small molecules. *Stem Cell Rep.* **8**, 538–547 (2017).
31. Guo, Z. Y. et al. In vivo direct reprogramming of reactive glial cells into functional neurons after brain injury and in an Alzheimer's disease model. *Cell Stem Cell* **14**, 188–202 (2014).
32. Heinrich, C. et al. Directing astroglia from the cerebral cortex into subtype specific functional neurons. *PLoS Biol.* **8**, e1000373 (2010).
33. Masserdotti, G. et al. Transcriptional mechanisms of proneural factors and REST in regulating neuronal reprogramming of astrocytes. *Cell Stem Cell* **17**, 74–88 (2015).
34. Zhang, L. et al. Small molecules efficiently reprogram human astroglial cells into functional neurons. *Cell Stem Cell* **17**, 735–747 (2015).
35. Heins, N. et al. Glial cells generate neurons: the role of the transcription factor Pax6. *Nat. Neurosci.* **5**, 308–315 (2002).
36. Qian, H. et al. Reversing a model of Parkinson's disease with in situ converted nigral neurons. *Nature* **582**, 550–556 (2020).

37. Zhou, H. et al. Glia-to-neuron conversion by CRISPR-CasRx alleviates symptoms of neurological disease in mice. *Cell* **181**, 590–603 (2020).
38. Mertens, J., Marchetto, M. C., Bardy, C. & Gage, F. H. Evaluating cell reprogramming, differentiation and conversion technologies in neuroscience. *Nat. Rev. Neurosci.* **17**, 424–437 (2016).
39. Huangfu, D. W. et al. Induction of pluripotent stem cells from primary human fibroblasts with only *Oct4* and *Sox2*. *Nat. Biotechnol.* **26**, 1269–1275 (2008).
40. Takahashi, K. et al. Induction of pluripotent stem cells from adult human fibroblasts by defined factors. *Cell* **131**, 861–872 (2007).
41. Banito, A. et al. Senescence impairs successful reprogramming to pluripotent stem cells. *Gene Dev.* **23**, 2134–2139 (2009).
42. Beausejour, C. M. et al. Reversal of human cellular senescence: roles of the p53 and p16 pathways. *EMBO J.* **22**, 4212–4222 (2003).
43. Hafner, A., Bulyk, M. L., Jambhekar, A. & Lahav, G. The multiple mechanisms that regulate p53 activity and cell fate. *Nat. Rev. Mol. Cell Biol.* **20**, 199–210 (2019).
44. Lancaster, M. A. & Knoblich, J. A. Generation of cerebral organoids from human pluripotent stem cells. *Nat. Protoc.* **9**, 2329–2340 (2014).
45. Bayraktar, O. A. et al. Astrocyte layers in the mammalian cerebral cortex revealed by a single-cell in situ transcriptomic map. *Nat. Neurosci.* **23**, 500–509 (2020).
46. Delile, J. et al. Single cell transcriptomics reveals spatial and temporal dynamics of gene expression in the developing mouse spinal cord. *Development* **146**, dev173807 (2019).
47. Yin, J. C. et al. Chemical conversion of human fetal astrocytes into neurons through modulation of multiple signaling pathways. *Stem Cell Rep.* **12**, 488–501 (2019).
48. Gascon, S., Masserdotti, G., Russo, G. L. & Gotz, M. Direct neuronal reprogramming: achievements, hurdles, and new roads to success. *Cell Stem Cell* **21**, 18–34 (2017).
49. Barkers, R. A., Gotz, M. & Parmar, M. New approaches for brain repair—from rescue to reprogramming. *Nature* **557**, 329–334 (2018).
50. Yang, H. et al. Sonic hedgehog effectively improves Oct4-mediated reprogramming of astrocytes into neural stem cells. *Mol. Ther.* **27**, 1467–1482 (2019).
51. Zhu, S. et al. Small molecules enable OCT4-mediated direct reprogramming into expandable human neural stem cells. *Cell Res.* **24**, 126–129 (2014).
52. Rosenzweig, E. S. et al. Restorative effects of human neural stem cell grafts on the primate spinal cord. *Nat. Med.* **24**, 484–490 (2018).

Acknowledgements

This study was supported by the National Key Research and Development Program of China (grant no. 2021ZD0202500), the National Natural Science Foundation of China (grant no. 32070956 to Z.S., grant nos. 32130044 and 31630029 to Y.S. and grant no. 32000680 to S.D.), the Fundamental Research Funds for Central Universities from Xiamen University (grant no. 20720180040 to Z.S.), the Natural Science Foundation of Shanghai (grant no. 20ZR1405200 to Z.S.), the MOE Frontiers Center for Brain Science Fund and the Starting Fund from Fudan University.

Author contributions

Z.S., J.X. and S.F. designed the experiments. J.X., S.F., Y.H. and Z.S. performed the astrocyte reprogramming, organoid analysis and transplantation. S.D. and S.F. conducted the electrophysiological studies. H.L. performed the single-cell RNA sequencing analysis. X.L., J.X. and S.F. isolated astrocytes from the patients. Z.S., J.X. and S.F. conducted the RNA sequencing analysis. Z.S., J.X., S.F. and S.D. wrote the manuscript and data interpretation. S.C. and Y.S. reviewed the data interpretation and manuscript content. Z.S. supported this study financially.

Competing interests

The authors declare no competing interests.

Additional information

Extended data is available for this paper at https://doi.org/10.1038/s41551-022-00963-6.

Supplementary information The online version contains supplementary material available at https://doi.org/10.1038/s41551-022-00963-6.

Correspondence and requests for materials should be addressed to Zhicheng Shao.

Peer review information *Nature Biomedical Engineering* thanks Qixin Chen, Woong Sun and Seungkwon You for their contribution to the peer review of this work. Peer reviewer reports are available.

Reprints and permissions information is available at www.nature.com/reprints.

Publisher's note Springer Nature remains neutral with regard to jurisdictional claims in published maps and institutional affiliations.

https://doi.org/10.1038/s41551-022-00963-6

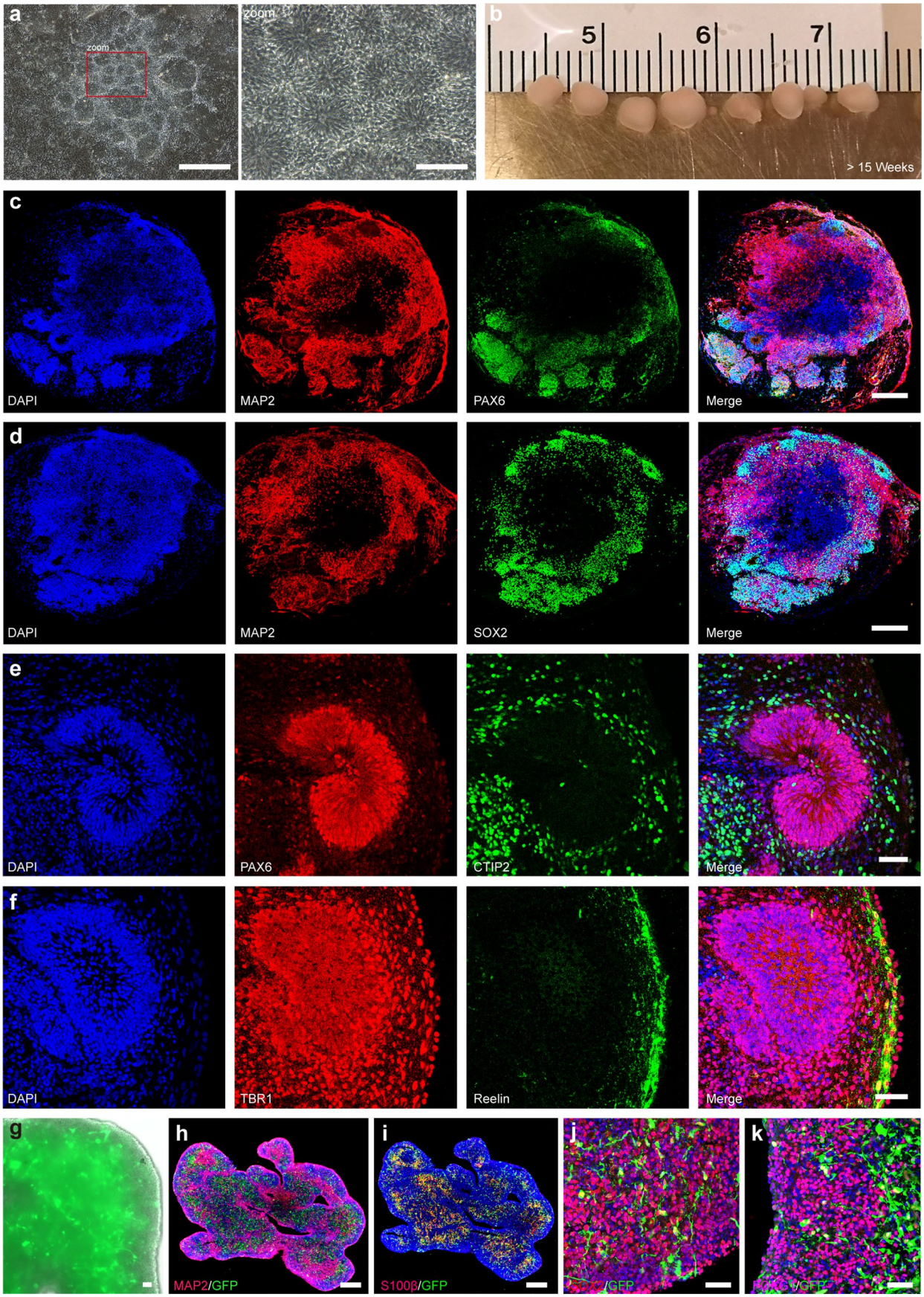

Extended Data Fig. 1 | See next page for caption.

https://doi.org/10.1038/s41551-022-00963-6

Extended Data Fig. 1 | Characterization of hAD-Organs. a, Phase images of Op53-CSBRY induced rosette-like clusters and the expanded red box (left) showing zoom-in images (right) of rosette-like clusters at 14 days. Scale bars, left: 400 µm, right: 100 µm. **b**, Phase image of hAD-Organs in suspension culture for over 15 weeks. **c - d**, Representative images of sections from hAD-Organs showing neuroepithelium-like structures at week 7. Showing neural progenitor marker SOX2 and PAX6, and neuronal marker MAP2. Scale bar, 250 µm. **e** and **f**, Immunostaining of $PAX6^+$, $CTIP2^+$ and $TBR1^+$ and $Reelin^+$ cells located in different cortical layers in 10-week-old hAD-Organs. Scale bar, 50 µm. **g**, Representive image of hGFAP::GFP and brightfield in 3-week-old cortical organoid (n = 3). Scale bar, 500 µm. **h - k**, Showing expression of MAP2, S100β, SOX2, and FOXG1 in 3-week-old cortical organoid. Scale bars, h and i: 500 µm, j and k: 50 µm. (Representative images from three sections of organoids with similar results (c-f, h-k).

https://doi.org/10.1038/s41551-022-00963-6

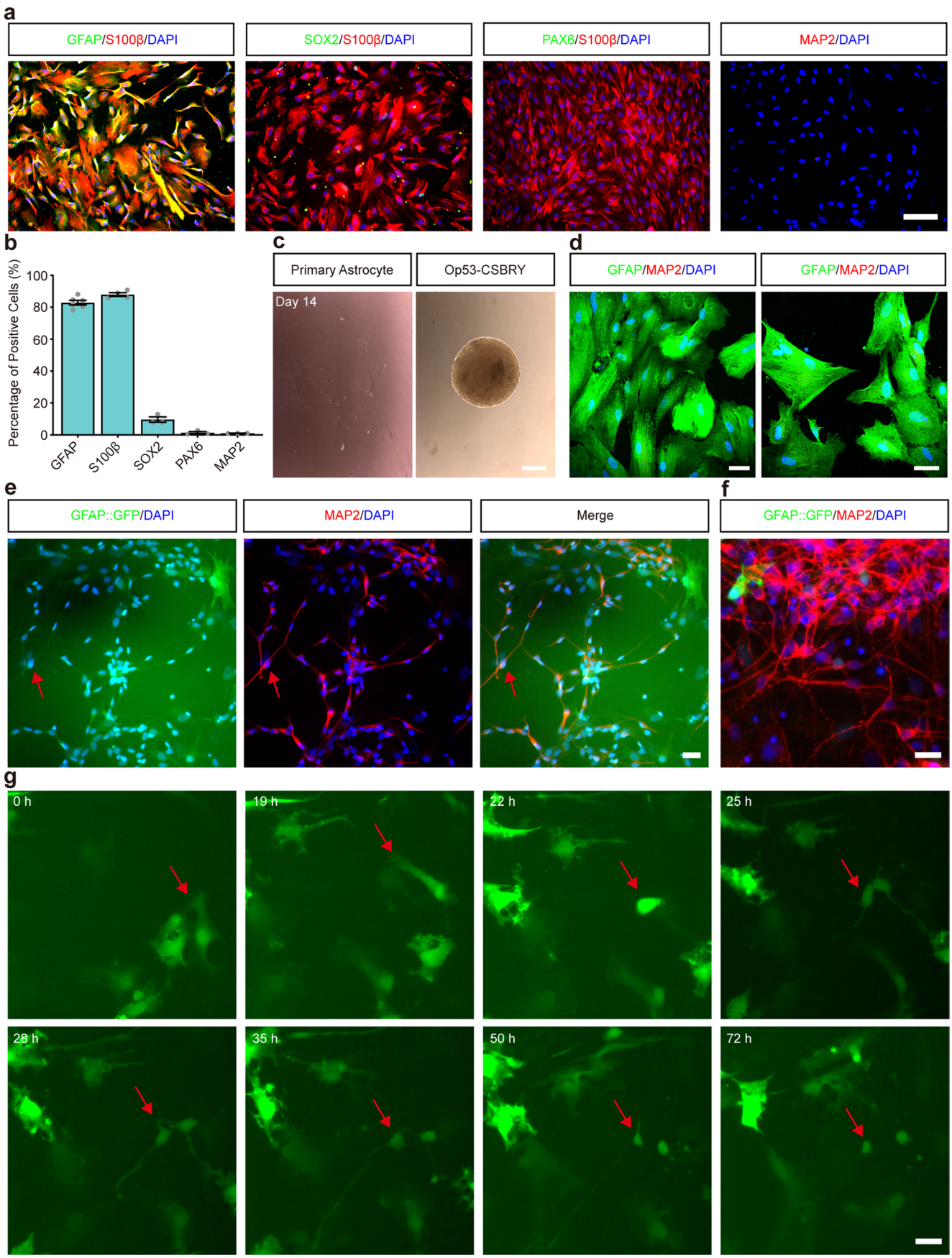

Extended Data Fig. 2 | See next page for caption.

https://doi.org/10.1038/s41551-022-00963-6

Extended Data Fig. 2 | Characterization of human astrocytes. a, Characterizing human primary astrocytes (HA1800) by immunostaining for GFAP, S100β, SOX2, PAX6 and MAP2. Scale bar, 100 µm. **b**, Quantitative analysis of the population of human primary astrocytes at several randomaly chosen fields per coverslip (n = 3 independent experiments). Data are presented as mean ± SEM. **c**, Neurosphere assay of human primary astrocytes comparing with Op53-CSBRY induced astrocytes. Scale bar, 200 µm. **d**, Immunostaining of primary human astrocytes with GFAP and MAP2 treated with either ISX-9 (10 µM) (left), or retinoic acid (RA, 100 nM) for 7 days respectively. Scale bars, 50 µm. **e**, Immunostaining for MAP2 after astrocytes induced by Op53-CSBRY and infected with hGFAP::GFP virus at day 7 (n = 3 independent experiments). Scale bars, 50 µm. **f**, Immunostaining for MAP2 in Op53-CSBRY induced astrocytes infected with hGFAP::GFP virus at day 26 (n = 3 independent experiments). Scale bar, 25 µm. **g**, Live cell tracking of the conversion of human astrocytes during Op53-CSBRY reprogramming. Scale bars, 25 µm.

https://doi.org/10.1038/s41551-022-00963-6

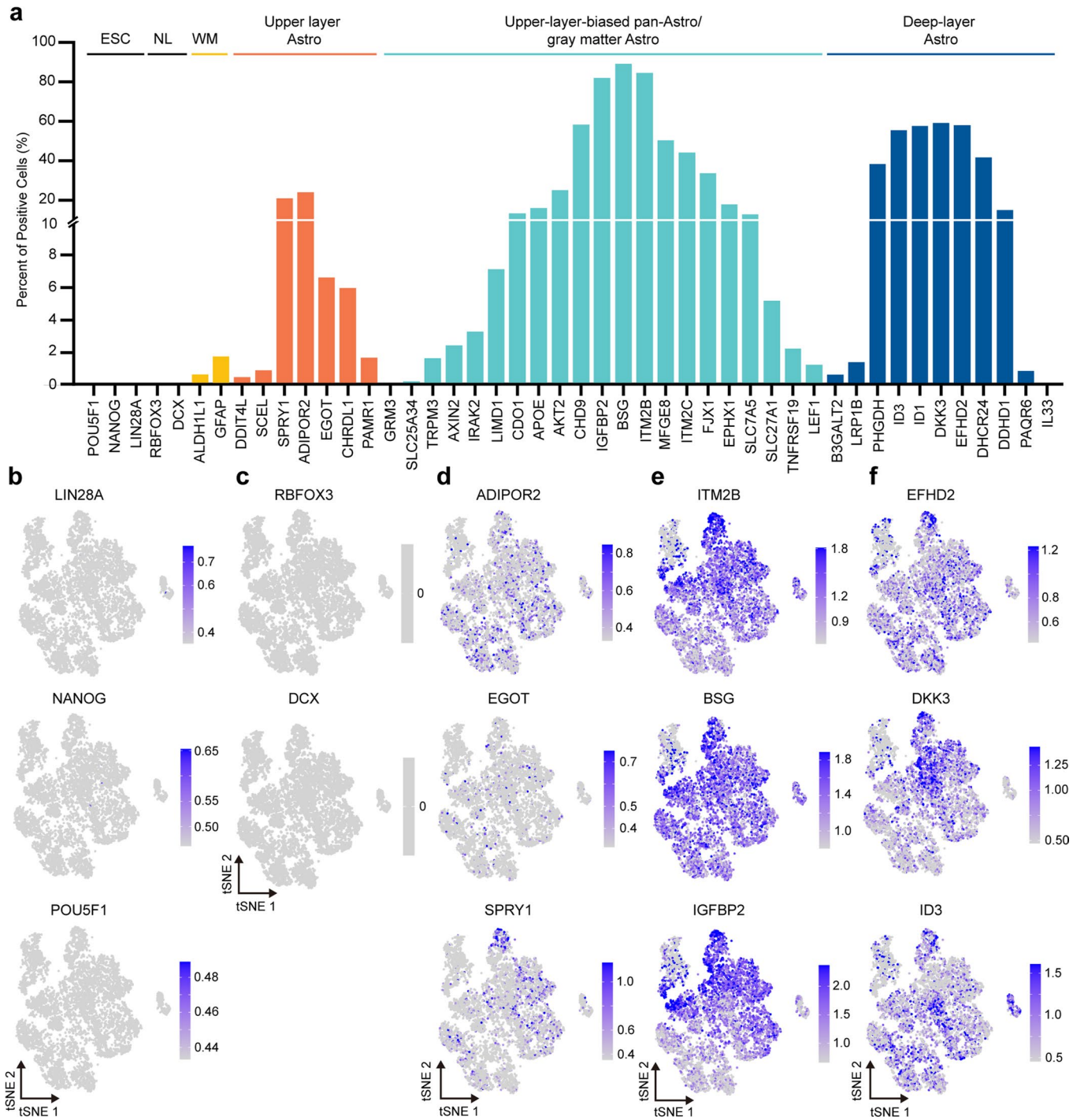

Extended Data Fig. 3 | Characterization of human astrocytes by single-cell RNA-sequencing. a, Graph showing cell percentage of expression of selected pluripotecy (ESC), neuron layer (NL), white matter (WM), upper layer astrocyte, upper-layer-biased pan-astrocyte/gray matter astrocyte and deep layer astrocyte related genes in brain cortical astrocytes. **b - f**, tSNE plots showing gene expression map of representative pluripotecy marker gene LIN28A, NANOG and POU5F1 (b), neuron gene RBFOX3 and DCX (c), upper layer astrocyte gene ADIPOR2, EGOT and SPRY1 (d), upper-layer-biased pan-astrocyte/gray matter astrocyte gene ITM2B, BSG and IGFBP2 (e), and deep layer astrocyte gene EFHD2, DKK3 and ID3 (f).

https://doi.org/10.1038/s41551-022-00963-6

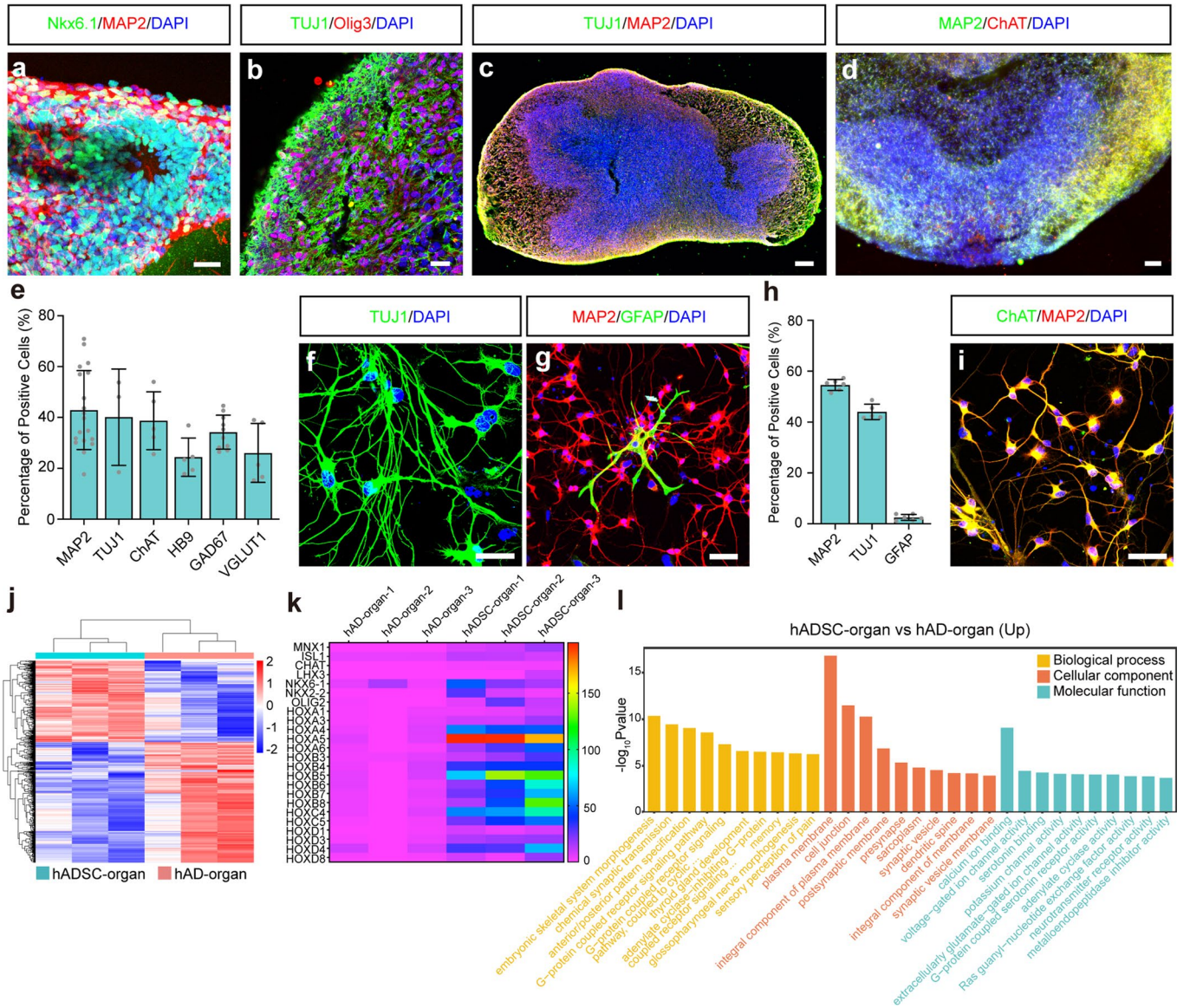

Extended Data Fig. 4 | Characterization of hADSC-Organs. a and **b**, Immunostaining images of dorsal and ventral pMN progenitor markers Nkx6.1 and Olig3 labeled with neuron markers. Scale bar, 25 μm. **c**, The horizontal plane image of sections from hADSC-Organs (representative images from three sections of spinal-cord organoids with similar results) stained for neural markers TUJ1 and MAP2. Scale bar, 200 μm. **d**, Image of spinal cord motor neuron ($ChAT^+/MAP2^+$) in 10-week-old hADSC-Organs (representative images from three sections of spinal-cord organoids with similar results). Scale bar, 100 μm. **e**, Quantitative analysis of neuronal subtypes of hADSC-Organs at week 10 stained for neuronal markers ChAT, HB9, GAD67 and VGLUT (n = 3 sections of organoids). **f** and **g**, Immunostaining of $GFAP^+$, $TUJ1^+$ and $MAP2^+$ cells in dissociated 10-week-old hADSC-Organs at several randomaly chosen fields per coverslip (n = 3 independent experiments). Scale bar, 50 μm. **h**, Quantitative the percentage of cells in dissociated 10-week-old hADSC-Organs for MAP2, TUJ1 and GFAP positive cells at several randomaly chosen fields per coverslip (n = 3 independent experiments). **i**, Representative images of $ChAT^+$ spinal motor neurons co-localized with $MAP2^+$ cells in dissociated 10-week-old hADSC-Organs at several randomaly chosen fields per coverslip (n = 3 independent experiments). Scale bar, 50 μm. **j** and **k**, Cluster analysis of differentially expressed genes show that the gene expression profile of hADSC-Organs was significantly different from that of hAD-Organs. The colour bar represents scaled gene expression value (j). Spinal cord specific markers MNX1, ChAT, ISL1, LHX3, Nkx6.1, NKX2.2 and HOX family were significantly high expression in hADSC-Organs. (n = 3 independent experiments). The colour bar represents FPKM value (k). **l**, KEGG Pathway enrichment assay demonstrating up-regulated genes comparing hADSC-Organs with hAD-Organs. Data are presented as mean ± SEM.

https://doi.org/10.1038/s41551-022-00963-6

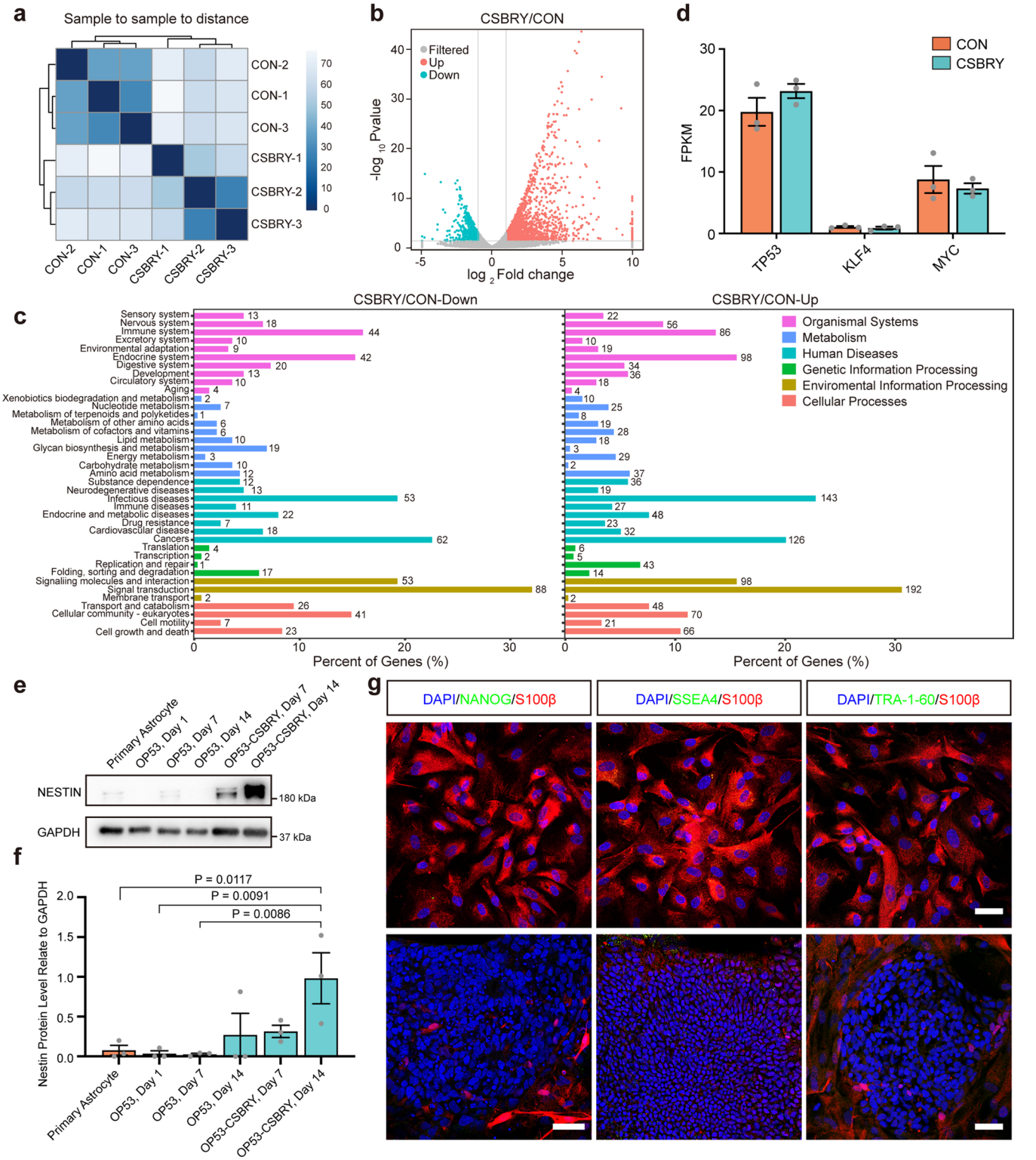

Extended Data Fig. 5 | Gene-expression profiles of astrocytes reprogrammed via Op53-CSBRY. a, Sample distance matrix showing three independent biological replicates treated by CSBRY. **b**,Volcano plots showing the results of RNA-seq after CSBRY/DMSO control treatment of Op53. Each dot represents a single gene, including upregulated, downregulated, and filtered genes. FDR ≤ 0.05 and $\log_2$FC > 1. **c**, Showing significantly different expression (DE) genes were regulated by CSBRY/DMSO control treatment of Op53. FDR ≤ 0.05 and $\log_2$FC > 1. **d**, CSBRY regulated the cancer genes TP53, KLF4 and MYC (n = 3 independent experiments). Multiple unpaired Student's t-test was used for comparing each groups. **e - f**, Gray scale image and quantification of Nestin protein expression in human primary astrocytes, OP53 control group at day 1, 7 and 14, and OP53-CSBRY treat group at day 7 and 14 (n = 3 independent experiments). Data are presented as mean ± SEM. Ordinary one-way ANOVA with Dunnett's multiple comparison test was used for multiple comparisons. **g**, Immunostaining of pluripotent markers of NANOG, SSEA4 and TRA-1-60 in human primary astrocyte (top row) and OP53-CSBRY treated cells (bottom row) at several randomaly chosen fields per coverslip (n = 3 independent experiments). Scale bar, 50 μm. Data are presented as mean ± SEM.

https://doi.org/10.1038/s41551-022-00963-6

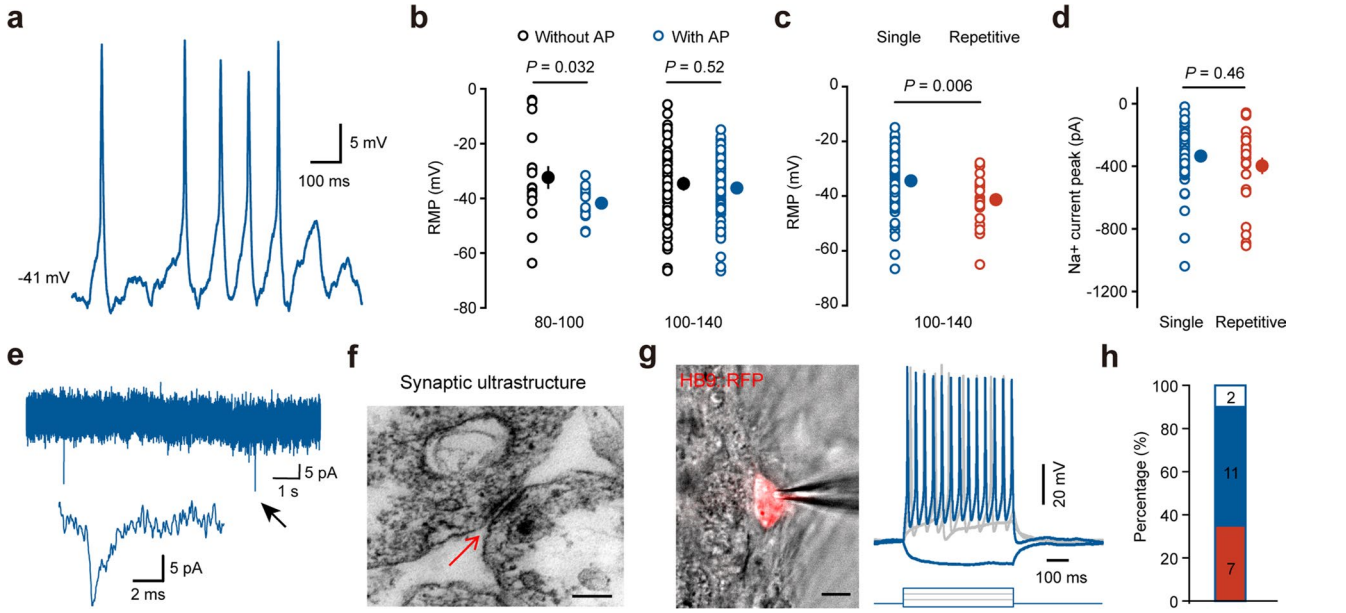

Extended Data Fig. 6 | Functional characterization of induced neurons from human astrocytes. a, Example trace showing spontaneous firing in the same cell shown in Fig. 7b. **b**, Group data comparing the RMP at different culture stages. For group 80-100 days: Without AP, n = 18 vs. With AP, n = 14; For 100-140 days: Without AP, n = 88 vs. With AP, n = 47. Data are presented as mean ± SEM. Two-sample Student's t-test was used for comparing with AP and without AP in each group. **c**, Group data comparing the RMP in cells with single AP and repetitive AP. Single AP: n = 65 vs. Repetitive AP: n = 23. Data are presented as mean ± SEM. Two-sample Student's t-test was used for comparing. **d**, Group data comparing the peak amplitudes of Na^+ currents. Single AP: n = 46 vs. Repetitive APs: n = 23. Data are presented as mean ± SEM. Mann-Whitney test was used for comparing between single and repetitive APs. **e**, An example current trace showing two spontaneously occurring putative postsynaptic currents (PSC). The second PSC event (arrow) was expanded for clarity (bottom). **f**, An example synaptic ultrastructure (red arrow) in 10-week-old hAD-Organs (n = 3 independent experiments). Scale bar, 100 nm. **g**, Left, merged image of IR-DIC and HB9::RFP positive of an example recorded cells isolated from 9-week-old hADSC-Organs (n = 3 independent experiments). Scale bar, 10 μm. Right, membrane potential responses (top) to intracellular injections of step currents (bottom). The blue traces indicate the responses to +50/−10 pA current pulses. **h**, The percentage of cells without AP (white), with single AP (blue) and repetitive AP (red) (top). The number of recorded cells in each group was provided.

https://doi.org/10.1038/s41551-022-00963-6

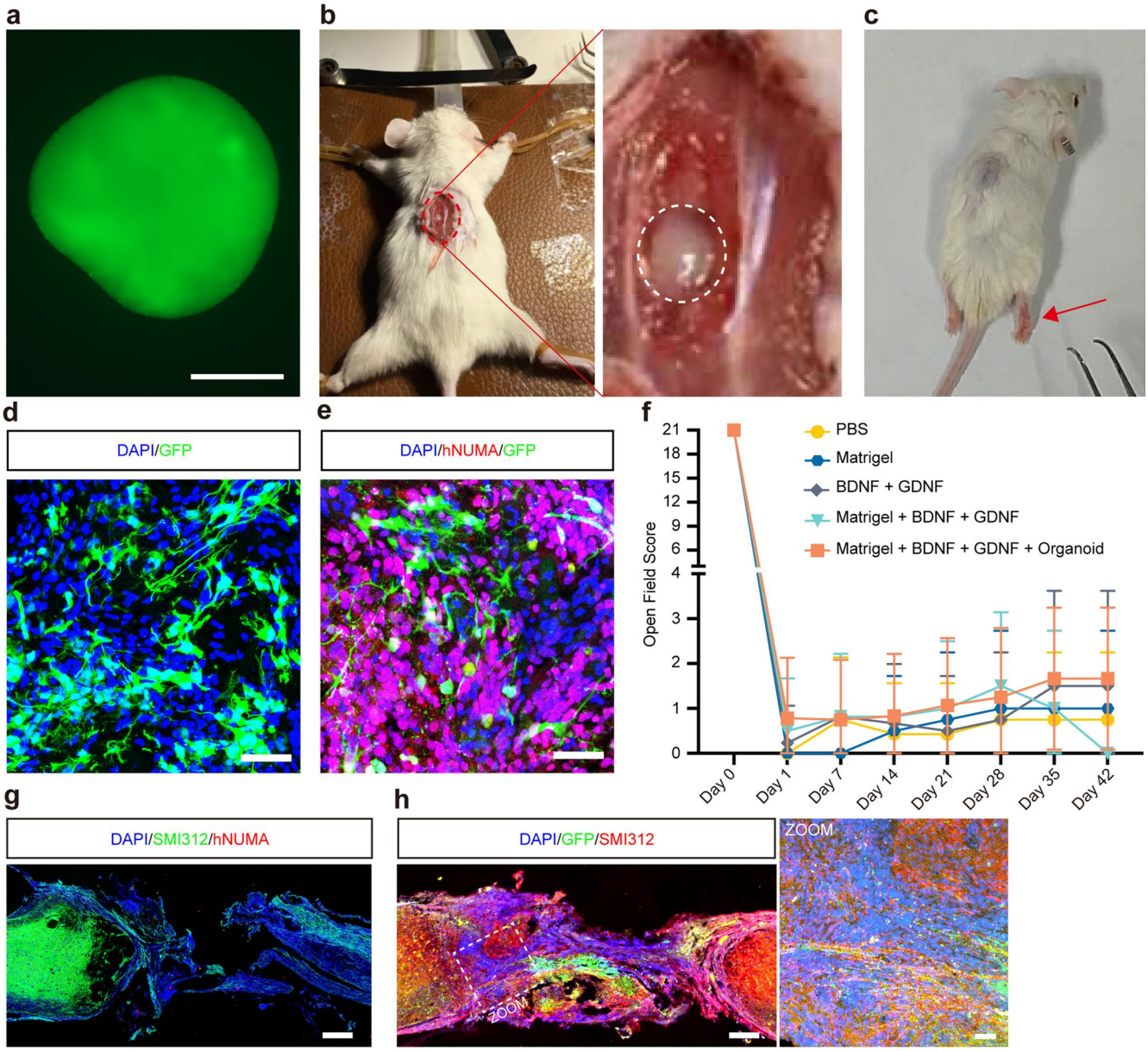

Extended Data Fig. 7 | Transplantation of hADSC-Organs into a complete spinal cord injury in NOD-SCID mice. a, Representative images of 7-week-old hADSC-Organs expressed high GFP after transduction with LV-Ubi-GFP virus infection (n = 25 organoids). Scale bar, 500 µm. **b**, The procedure of hADSC-Organs transplantation showing the site of the spinal cord amputation. **c**, The posterior soles of mice with complete spinal cord injury showed hindlimb paralysis with the valgus phenomenon. **d**, Representative images survival of GFP$^+$ cells in grafted hADSC-Organs in mice (n = 3). Scale bar, 50 µm. **e**, Representative images survival of GFP$^+$ cells in the grafted field of hADSC-Organs were human nuclei positive of hNUMA (n = 3 independent experiments). Scale bar, 50 µm. **f**, Open field score of grafted hADSC-Organs mice with 5 different treatments. The number of experiments (n) are summarized in Supplementary Table 1. Each treatment for 10–25 mice and in total 5 groups for 70 mice. Data are presented as mean ± SEM. **g** and **h**, Representative images of the spinal cord from **g**, the Matrigel only group and **h**, hADSC-Organs +MBG group and an expanded image of the outlined region (white box) where the hADSC-Organs were implanted (n = 3 mice). Scale bars, g: 250 µm, h: left, 250 µm, right, 50 µm.

nature portfolio

Corresponding author(s): Zhicheng Shao

Last updated by author(s): Apr 9, 2022

Reporting Summary

Nature Portfolio wishes to improve the reproducibility of the work that we publish. This form provides structure for consistency and transparency in reporting. For further information on Nature Portfolio policies, see our Editorial Policies and the Editorial Policy Checklist.

Statistics

For all statistical analyses, confirm that the following items are present in the figure legend, table legend, main text, or Methods section.

n/a	Confirmed
☐	☒ The exact sample size (*n*) for each experimental group/condition, given as a discrete number and unit of measurement
☐	☒ A statement on whether measurements were taken from distinct samples or whether the same sample was measured repeatedly
☐	☒ The statistical test(s) used AND whether they are one- or two-sided *Only common tests should be described solely by name; describe more complex techniques in the Methods section.*
☐	☒ A description of all covariates tested
☐	☒ A description of any assumptions or corrections, such as tests of normality and adjustment for multiple comparisons
☐	☒ A full description of the statistical parameters including central tendency (e.g. means) or other basic estimates (e.g. regression coefficient) AND variation (e.g. standard deviation) or associated estimates of uncertainty (e.g. confidence intervals)
☐	☒ For null hypothesis testing, the test statistic (e.g. *F*, *t*, *r*) with confidence intervals, effect sizes, degrees of freedom and *P* value noted *Give P values as exact values whenever suitable.*
☒	☐ For Bayesian analysis, information on the choice of priors and Markov chain Monte Carlo settings
☐	☒ For hierarchical and complex designs, identification of the appropriate level for tests and full reporting of outcomes
☒	☐ Estimates of effect sizes (e.g. Cohen's *d*, Pearson's *r*), indicating how they were calculated

Our web collection on statistics for biologists contains articles on many of the points above.

Software and code

Policy information about availability of computer code

Data collection

All the immunostaining images were taken using a Leica TCS SP8. Image J software (Version 1.51p, NIH, Bethesda, MD) was used to adjust colour balance. All the traced neuronal images were taken using the Zesi TE-2000-S. Grids were analysed using an HT-7800 transmission electron microscope (Hitachi). Cell populations were analyzed Beckman Gallios flow cytometer. Data analysis was performed using FlowJo software. The libraries were sequenced on an Illumina HiSeq X Ten platform and 150 bp paired-end reads were generated. Raw data (raw reads) of fastq format were firstly processed using Trimmomatic, about 40–65M raw reads for each sample were generated. Single-cell RNA-seq were performed using 10x Genomics to classify subtypes of human astrocytes and populations of human-astrocyte-derived spinal-cord organoids (hADSC-organs). Illumina NovaSeq6000 was used to obtain paired-end 150 bp reads. The obtained reads were aligned to the human reference genome (GRCh38) using Cell Ranger. Then, filtering barcodes and UMI counting were conducted. An infrared-differential interference contrast (IR-DIC) microscope (BX-51WI, Olympus) was used for the visualization of culture cells. A Multiclamp 700B amplifier (Molecular Devices) and a Power1401-3A analog-to-digital converter were used for whole-cell patch-clamp recordings.

Data analysis	Unpaired two-tail t-tests using GraphPad Prism software version 7.0 were used to determine statistical significance. Spike2 and Signal software (Cambridge Electronic Design) together with MATLAB (MATHWORKS) were used for data analyses. Behavioural analyses were evaluated by two observers with a double-blind approach according to the BBB-score criteria. The clean reads were mapped to the human genome using HISAT2. The FPKM value of each gene was calculated using Cufflinks, and the read counts of each gene were obtained by HTSeq-count. Differential expression analysis was performed using the DESeq (2012) R package. Hierarchical cluster analysis of differentially expressed genes (DEGs) was performed to explore gene-expression patterns. GO enrichment and KEGG pathway-enrichment analysis of DEGs were performed, respectively, using R based on the hypergeometric distribution. The gene expression of cells at the single-cell level was normalized using a global-scaling normalization method (normalization.method =''LogNormalize,'') and scaled using the R package Seurat (scale.factor = 10,000). To do principal component analysis (PCA), the top-1,500 high-variable genes were selected and scaled. The top-20 principal components were used to construct the nearest-neighbour graph using FindNeighbors, and clusters cells were identified by function FindClusters with a resolution of 0.8 in Seurat.

For manuscripts utilizing custom algorithms or software that are central to the research but not yet described in published literature, software must be made available to editors and reviewers. We strongly encourage code deposition in a community repository (e.g. GitHub). See the Nature Portfolio guidelines for submitting code & software for further information.

Data

Policy information about availability of data

All manuscripts must include a data availability statement. This statement should provide the following information, where applicable:

- Accession codes, unique identifiers, or web links for publicly available datasets
- A description of any restrictions on data availability
- For clinical datasets or third party data, please ensure that the statement adheres to our policy

The data supporting the results in this study are available within the paper and its Supplementary Information. The RNA-seq data are available from the Gene Expression Omnibus (GEO) database via the accession number GSE168635. The raw single-cell RNA-sequencing data are available from the Genome Sequence Archive (GSA) database via the accession number HRA002541.

Field-specific reporting

Please select the one below that is the best fit for your research. If you are not sure, read the appropriate sections before making your selection.

☒ Life sciences ☐ Behavioural & social sciences ☐ Ecological, evolutionary & environmental sciences

For a reference copy of the document with all sections, see nature.com/documents/nr-reporting-summary-flat.pdf

Life sciences study design

All studies must disclose on these points even when the disclosure is negative.

Sample size	No statistical methods were used to predetermine sample sizes.
Data exclusions	No data were excluded.
Replication	All attempts at replication were successful.
Randomization	Organoids were randomly selected prior to immunostaining, MEA recording, electron microscopy, transplantation, RNA-seq and single-cell RNA-sequencing. Mice were randomly assigned to experimental and control groups.
Blinding	Blinding was used during cell counting. Locomotor scores for the mice were also determined in a double-blinded manner.

Reporting for specific materials, systems and methods

We require information from authors about some types of materials, experimental systems and methods used in many studies. Here, indicate whether each material, system or method listed is relevant to your study. If you are not sure if a list item applies to your research, read the appropriate section before selecting a response.

Materials & experimental systems

n/a	Involved in the study
☐	☒ Antibodies
☐	☒ Eukaryotic cell lines
☒	☐ Palaeontology and archaeology
☐	☒ Animals and other organisms
☐	☒ Human research participants
☒	☐ Clinical data
☒	☐ Dual use research of concern

Methods

n/a	Involved in the study
☒	☐ ChIP-seq
☐	☒ Flow cytometry
☒	☐ MRI-based neuroimaging

Antibodies

Antibodies used

anti-MAP2 (Cell Signaling Technology, 4542S, 1:1,000), anti-GFAP (Millipore, MAB360, 1:500), anti-S100 beta (Abcam, ab52642, 1:200), anti-SOX2 (BD Pharmingen, 561469, 1:50), anti-PAX6 (Biolegend, 901301, 1:300), anti-TUJ1 (Biolegend, B209227, 1:1,000), anti-NKX6.1 (DSHB, F55A12, 1:50), anti-Olig-2 (Millipore, AB9610, 1:200), anti-OLIG3 (Sigma, HPA018303, 1:25), anti-VGlut1 (UC Davids/NIH NeuroMab Facility, 75-066, 1:250), anti-HB9 (DSHB, 81.5C10, 1:4), anti-ChAT (Millipore, AB144P, 1:100), anti-GABA (Immunostar, 20094, 1:50), anti-Ctip2 (Abcam, ab18465, 1:500), anti-SATB2 (Abcam, ab34735, 1:500), anti-GAD67 (Millipore, MAB5406, 1:50), anti-Bassoon (Abcam, ab82958, 1:200), anti-Synaptophysin (Novus, NBP1-19222, 1:500), anti-hNuMA (Abcam, ab97585, 1:200), anti-GFP (Thermo, MA5-15256, 1:250), anti-GFP (Cell Signaling Technology, 2956S, 1:500), anti-Oct3/4 (BD Pharmingen, 561555, 1:1,000), anti-p53 (Epitomics, 1026-1, 1:300), anti-Brn2 (GeneTex, GTX114650, 1:1,000), anti-Reelin (MBL, D223-3, 1:300), anti-TBR1 (Abcam, ab31940, 1:1,000), anti-FOXG1 (Abcam, ab196868, 1:1,00), anti-SMI 312 (Biolegend, 837904, 1:500), anti-Nestin (Abcam, ab22035, 1:2000).

Validation

The antibodies were validated by the manufacturers. List of each antibody manufacturer's website:
anti-MAP2 (https://www.labome.com/product/Cell-Signaling-Technology/4542S.html#:~:text=Established%20in%20Beverly%2C%20MA%20in%201999%2C%20Cell%20Signaling,help%20define%20mechanisms%20underlying%20cell%20function%20and%20disease.)
anti-GFAP (https://www.merckmillipore.com/CN/zh/product/Anti-Glial-Fibrillary-Acidic-Protein-Antibody-clone-GA5,MM_NF-MAB360?ReferrerURL=https%3A%2F%2Fcn.bing.com%2F&bd=1)
anti-S100 beta (https://www.abcam.com/s100-beta-antibody-ep1576y-astrocyte-marker-ab52642.html)
anti-SOX2 (https://www.bdbiosciences.com/zh-cn/products/reagents/flow-cytometry-reagents/research-reagents/single-color-antibodies-ruo/purified-mouse-anti-sox2.561469)
anti-PAX6 (https://www.labome.com/product/BioLegend/901301.html)
anti-TUJ1 (https://www.biolegend.com/en-us/products/purified-anti-tubulin-beta-3-tubb3-antibody-11580?GroupID=GROUP686)
anti-NKX6.1 (https://dshb.biology.uiowa.edu/F55A12)
anti-Olig-2 (https://www.merckmillipore.com/CN/zh/product/Anti-Olig-2-Antibody,MM_NF-AB9610?ReferrerURL=https%3A%2F%2Fcn.bing.com%2F&bd=1)
anti-OLIG3 (https://www.sigmaaldrich.cn/CN/zh/search/hpa018303?focus=products&page=1&perPage=30&sort=relevance&term=HPA018303&type=product)
anti-VGlut1 (https://neuromab.ucdavis.edu/neuromabs.cfm)
anti-HB9 (https://dshb.biology.uiowa.edu/81-5C10)
anti-ChAT (https://www.merckmillipore.com/CN/zh/product/Anti-Choline-Acetyltransferase-Antibody,MM_NF-AB144P?ReferrerURL=https%3A%2F%2Fcn.bing.com%2F&bd=1)
anti-GABA (https://www.labome.com/product/ImmunoStar/20094.html)
anti-Ctip2 (https://www.abcam.com/ctip2-antibody-25b6-ab18465.html)
anti-SATB2 (https://www.abcam.com/SATB2-antibody-ab34735.html)
anti-GAD67 (https://www.merckmillipore.com/CN/zh/product/Anti-GAD67-Antibody-clone-1G10.2,MM_NF-MAB5406?ReferrerURL=https%3A%2F%2Fcn.bing.com%2F&bd=1)
anti-Bassoon (https://www.abcam.com/bassoonbsn-antibody-sap7f407-ab82958.html)
anti-Synaptophysin (https://www.novusbio.com/products/synaptophysin-antibody-ep10_nbp1-19222)
anti-hNuMA (https://www.abcam.com/NuMA-antibody-ab97585.html)
anti-GFP (https://www.thermofisher.cn/cn/zh/antibody/product/GFP-Antibody-clone-GF28R-Monoclonal/MA5-15256)
anti-GFP (https://www.cellsignal.cn/products/primary-antibodies/gfp-d5-1-rabbit-mab/2956)
anti-Oct3/4 (https://www.bdbiosciences.com/en-us/products/reagents/flow-cytometry-reagents/research-reagents/single-color-antibodies-ruo/purified-mouse-anti-oct3-4-human-isoform-a.561555)
anti-p53 (https://www.biomart.cn/infosupply/2931375.htm)
anti-Brn2 (https://www.genetex.cn/Product/Detail/Brn2-antibody/GTX114650)
anti-Reelin (https://www.mblbio.com/bio/g/dtl/A/?pcd=D223-3)
anti-TBR1 (https://www.abcam.com/tbr1-antibody-ab31940.html)
anti-FOXG1 (https://www.abcam.cn/foxg1-antibody-epr18987-ab196868.html)
anti-SMI 312 (https://www.biolegend.com/en-gb/products/purified-anti-neurofilament-marker-pan-axonal-cocktail-12811?Clone=SMI%20312)
anti-Nestin (https://www.abcam.com/nestin-antibody-10c2-neural-stem-cell-marker-ab22035.html)

Eukaryotic cell lines

Policy information about cell lines

Cell line source(s)	Human astrocytes isolated from human brain cerebral cortex (Catalog #1800, Sciencell), H9 human embryonic stem cells (WiCell).
Authentication	The cells were immunostained with the astrocyte markers GFAP and S100b.
Mycoplasma contamination	All cell lines were routinely tested for mycoplasma contamination. The cell lines used in this study were verified to be mycoplasma-free before undertaking any experiments with them.
Commonly misidentified lines (See ICLAC register)	No commonly misidentified cell lines were used.

Animals and other organisms

Policy information about studies involving animals; ARRIVE guidelines recommended for reporting animal research

Laboratory animals	We used over-6 weeks-old Nod Scid mice for transplantation, 7–12-weeks-old mice for for BBB-score behavioural testing, and 12-weeks-old mice for immunohistochemistry.
Wild animals	The study did not involve wild animals.
Field-collected samples	The study did not involve samples collected from the field.
Ethics oversight	All experimental protocols were approved by the Institutional Animal Care and Use Committee at Xiamen University.

Note that full information on the approval of the study protocol must also be provided in the manuscript.

Human research participants

Policy information about studies involving human research participants

Population characteristics	13–65 years-old patients with gliomas sided to the focal lesion tissue.
Recruitment	Human healthy brain tissues adjacent to gliomas were obtained with written consent from patients at Zhongshan Hospital.
Ethics oversight	The protocol involving human mature astrocytes was approved by the scientific research subcommittee of the medical ethics committee of Zhongshan hospital affiliated to Xiamen University.

Note that full information on the approval of the study protocol must also be provided in the manuscript.

Flow Cytometry

Plots

Confirm that:

☒ The axis labels state the marker and fluorochrome used (e.g. CD4-FITC).

☒ The axis scales are clearly visible. Include numbers along axes only for bottom left plot of group (a 'group' is an analysis of identical markers).

☒ All plots are contour plots with outliers or pseudocolor plots.

☒ A numerical value for number of cells or percentage (with statistics) is provided.

Methodology

Sample preparation	Astrocytes (HA1800) were transfected with plasmid, and then treated with CHIR99021, SB431542, RepSox and Y27632, or without treatment, 3 days after transfection. Cells were isolated using TrypLE and fixed by 4% PFA for 15 min, washed three times with PBS, and then resuspended in PBS buffer containing 2% normal serum (FACS buffer).
Instrument	Beckman Gallios flow cytometer.
Software	Data analysis was performed using FlowJo.
Cell population abundance	All the cells in culture plate were dissociated, stained with and without primary antibodies, and sorted. The purity was determined by MAP2 staining.

Gating strategy

All samples were preliminarily gated by FSC and SSC to select singlet cells. The boundary of positive and negative populations was determined by the FITC-IgG intensity of cells stained without primary antibody.

☒ Tick this box to confirm that a figure exemplifying the gating strategy is provided in the Supplementary Information.